formaldehyde, permeabilized in 0.1% saponin, and stained with FITC conjugated anti-perforin mAb or anti-granzyme B mAb or isotype control IgG2a. Figure shows the dot plot of the gated $CD8^+$ T cells. The right hand quadrant shows $CD8^{high}$ T cells (activated $CD8^+$ T cells) and the number indicates the percentage of perforin or granzyme B positive T cells among gated $CD8^{high}$ T cells. *To determine whether direct interaction between $CD4^+$ and $CD8^+$ T cells for perforin and granzyme B production from $CD8^+$ T cells, is needed, $CD4^+$ T cells were cultured in inserts in a 24-well plate, and were not allowed to interact directly with $CD8^+$ T cells. As a control experiment, exogenous IL-2 (in the left hand dot plot) at a concentration of 50 U/ml was added to $CD8^+$ T cells. (**B**) Enhanced expression of perforin and granzyme B from $CD4^+$ T cells. The right hand quadrant shows $CD4^{high}$ T cells, and the number indicates percentage of $CD4^{high}$ T cells producing perforin and granzyme B. (**C**) Enhanced expression of granulysin from $CD8^+$ and $CD4^+$ T cells, co-cultured with LipoK and *M. leprae* stimulated DCs. The protocol was followed as per the staining of perforin, except that the surface stain used was FITC conjugated-CD4 and APC conjugated anti-CD8 mAb, and subsequently PE conjugated granulysin was used. Figure shows the dot plot of the gated $CD8^+$ and $CD4^+$ T cells. The right hand quadrant shows $CD8^{high}$ or $CD4^{high}$ T cells (activated T cells) and the number indicates the percentage of granulysin positive T cells among gated $CD8^{high}$ and $CD4^{high}$ T cells. Representative data of three separate experiments with different donors is shown.

doi:10.1371/journal.pntd.0001401.g004

antibody could almost totally inhibit the IL-12 production from DCs, as well as the T cell activating function of DCs (not shown), probably through blocking of the classical NF-kB pathway. Indeed, parthenolide, one of the major sesquiterpene lactones, known to inhibit NF-kB activity [24], inhibited the IL-12 production from DCs stimulated with *M. leprae* and LipoK. Also, IL-12 was efficiently produced when *M. leprae* was viable and not dead. Thus, although the exact mechanisms remain to be elucidated, some cell surface molecules and secreted components of *M. leprae* are responsible for the production of IL-12, which further modulates type 1 T cell responses [32,33].

A number of mechanisms are known to be involved in the clearance of intracellular bacteria, such as IFN-γ release, apoptosis induction of the macrophages and anti-microbial activity of CTL [12,15]. Production of IFN-γ could boost the ability to kill pathogens in host cells. In fact, it was found that LipoK activated *M. leprae* infected DCs, highly stimulated both memory $CD4^+$ and $CD8^+$ T cells, as well as naïve $CD4^+$ to produce IFN-γ, and further assisted in the proliferation of both T cell subsets (Fig. 3).

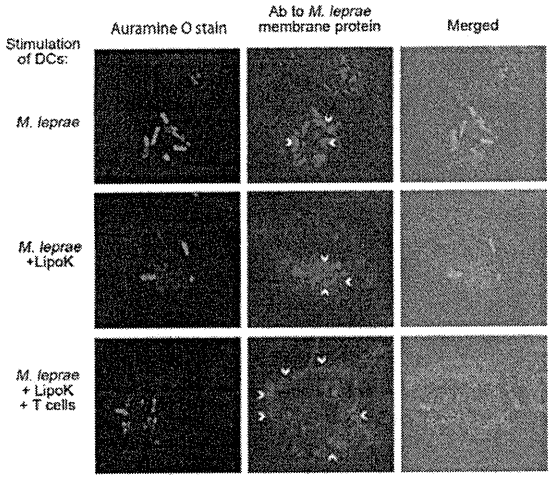

Figure 5. Localization of the membrane components of *M. leprae* at the periphery of the DCs. DCs were infected with either *M. leprae* alone or further stimulated with LipoK for 2 days and in some cases co-cultured with T cells. After 3 days co-culture with T cells, cover glass with attached DCs were fixed and observed under confocal microscopy-LSM5 Exciter. *M. leprae* was stained with Auramine O (shown in green) and *M. leprae* membrane components were stained with polyclonal rabbit antibody raised against the membrane fraction of *M. leprae* (depicted in red fluorescence). Alexa Fluor 633 conjugated anti-rabbit antibody (Molecular Probes) was used as the secondary antibody. Arrowheads indicate the positively stained region. Experiments were performed twice with different donors.

doi:10.1371/journal.pntd.0001401.g005

Inhibition of MHC class I and class II molecules on DCs, indicated that the activation of these T cells were MHC class II- and class I-dependent in $CD4^+$ T cell and $CD8^+$ T cells respectively. Further, proteolytic processing of *M. leprae* antigens was probably enhanced by LipoK treatment of DCs, since incubation with anti-*M. leprae* membrane Ab showed positive staining at the periphery of DCs, when co-cultured with T cells (Fig. 5). In addition, preliminary results showed that expression of MHC class I and II molecules on LipoK activated DCs, were elevated in those co-cultured with T cells. Thus, LipoK could probably assist in the processing and presentation of *M. leprae* antigens, and thereby, highly activate T cells.

The other important parameter, for the clearance of mycobacteria from the host cell, is their potential to activate antimicrobial effector mechanisms in human T cells. DCs have been shown to be involved in CTL induction following uptake of antigenic particles [25,34,35,36]. $CD8^+$ T cells co-cultured with LipoK

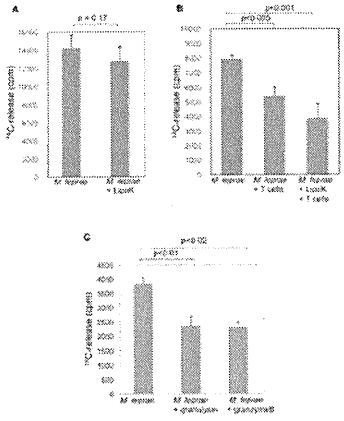

Figure 6. Reduction in the viability of *M. leprae* in DCs after co-culture with T cells and LipoK stimulation. (**A**) DCs were infected with *M. leprae* and stimulated with LipoK, 2 days later, cells were collected and the viability of *M. leprae* in DCs was measured by the radiorespirometric assay (metabolic CO_2 release) as described in Materials and Methods. In brief, ^{14}C labeled palmitic acid was added to the lysates of DCs and cultured at 33°C. After 7 days of culture, the amount of $^{14}CO_2$ evolved was measured using a Packard 1500 TRI-CARB liquid scintillation analyzer. (**B**) DCs were infected with *M. leprae* as in **A**, and co-cultured with T cells. Six days after the co-culture, DCs were lysed, and the viability of *M. leprae* was determined by the radiorespirometric assay. (**C**) *M. leprae* at a concentration of 1×10^7/well/200 µl in Middlebrook 7H9 media was incubated with granulysin or granzyme B for a period of 3 days at 33°C, and the viability determined as described in **A**. Unpaired Student's t test was used to find the statistical significance of the two sets of data. Representative data of three separate experiments is shown.

doi:10.1371/journal.pntd.0001401.g006

stimulated *M. leprae*-infected DCs, through $CD4^+$ T cells' help produced increased amount of cytolytic effector molecules: perforin and granzyme B. Adequate production of these cytolytic proteins from $CD8^+$ T cells required direct contact with $CD4^+$ T cells. Recently, there are studies that certain types of $CD4^+$ T cells possess direct cytotoxic potential [25,37,38]. We observed a portion of $CD4^{high}$ T cells (activated T cells), have the capacity to produce cytotoxic granules. Bastian et al. demonstrated that native *M. tuberculosis* heterogenous lipopeptides are potent immunogens for primary human T cells, and those T cells were $CD4^+$ and MHC class II restricted, challenging the current concepts that cytotoxic T cells were restricted to $CD8^+$ T cell subset [25]. Another lytic molecule, present in cytotoxic granules of T cells, is granulysin, which is reported to have direct anti-bacterial activity. Reports have shown the ability of T cells to secrete granulysin at the site of *M. leprae* infection, which provides evidence that anti-microbial activity of granule containing T cells is a mechanism of host defense in leprosy [39,40]. We observed that LipoK stimulated, *M. leprae* infected DCs, highly enhanced the production of granulysin from $CD8^+$ T cells. Unexpectedly, we observed that the percentage of $CD4^+$ T cells producing granulysin was higher than $CD8^+$ T cells. But, this fact was in lines with the earlier data, which showed co-localization of granulysin and $CD4^+$ T cells in tuberculoid leprosy lesions [39,40]. Thus, granulysin release by LipoK-mediated activation process, may lead to a direct anti-microbial effector pathway of host defense. These data demonstrated that both $CD4^+$ T cells and $CD8^+$ T cells, contribute to the induction of intracellular killing of *M. leprae*. These speculations were further supported by the fact that 50% of the phagocytosed bacilli were killed when infected DCs stimulated with LipoK, were co-cultured with T cells. This is the first observation of killing of *M. leprae* in an *ex vivo* system using human DCs and T cells. To further provide evidence of the effector mechanism at work during *M. leprae* killing by CTL, the direct effect of granulysin on *M. leprae* killing *in vitro* was analyzed. Results indicated that about 40% of *M. leprae* was killed by granulysin. Granulysin could probably lyse *M. leprae* by binding to the lipidic cell wall, through the same mechanism by which *M. tuberculosis* is destroyed by granulysin. Since, perforin is an essential molecule in the killing of intracellular *M. tuberculosis* [16], similar operation may be involved in intracellular *M. leprae* killing since perforin was effectively produced by T cells in our CTL culture system. On the other hand, direct killing of mycobacteria by granzymes is not known. But the viability of *M. leprae* was significantly lowered by granzyme B. Since granzyme B is one of the serine proteases that can target cytosolic and nuclear substrates to induce host cell death through mitochondrial perturbation, it may be involved in destroying the cell wall architecture of *M. leprae* by still unknown mechanism [41,42]. The contribution of the cytotoxic granules to killing of bacteria remains to be of interest for further investigation. Together, the results indicate that LipoK could contribute to protective host response against leprosy and eventually kill the bacteria, through the production of perforin, granulysin and granzyme B in T cells.

Acknowledgments

We appreciate the helpful assistance of Drs. Masanori Matsuoka and Masaichi Gidoh for the *M. leprae* propagation and isolation. Technical help for ELISA was kindly provided by Yukie Harada, Mizuho Kujiraoka, and Kumiko Matsubara for the isolation of PBMCs. We also thank the Japanese Red Cross Society for kindly providing the whole blood cells from healthy donors.

Author Contributions

Conceived and designed the experiments: YM TT YF MM. Performed the experiments: YM TT YF. Analyzed the data: YM TT TM MK MM. Contributed reagents/materials/analysis tools: YM TM MK. Wrote the paper: YM TT MM.

References

1. World Health Organization (2010) Global leprosy situation. Weekly epidemiological record 35: 337–348.
2. Ridley DS, Jopling WH (1966) Classification of leprosy according to immunity. A five-group system. Int J Lepr Other Mycobact Dis 34: 255–273.
3. Kaplan G, Cohn ZA (1986) The immunobiology of leprosy. Int Rev Exp Pathol 28: 45–78.
4. Maeda Y, Makino M, Crick DC, Mahapatra S, Srisungnam S, et al. (2002) Novel 33-kilodalton lipoprotein from *Mycobacterium leprae*. Infect Immun 70: 4106–4111.
5. Yamashita Y, Maeda Y, Takeshita F, Brennan PJ, Makino M (2004) Role of the polypeptide region of a 33 kDa mycobacterial lipoprotein for efficient IL-12 production. Cell Immunol 229: 13–20.
6. Tschumi A, Nai C, Auchli Y, Hunziker P, Gehrig P, et al. (2009) Identification of apolipoprotein n-acyltransferase (LNT) in mycobacteria. J Biol Chem 284: 27146–27156.
7. Pecora ND, Gehring AJ, Canaday DH, Boom WH, Harding CV (2006) *Mycobacterium tuberculosis* LprA is a lipoprotein agonist of TLR2 that regulates innate immunity and APC function. J Immunol 177: 422–429.
8. Krutzik SR, Ochoa MT, Sieling PA, Uematsu S, Ng YW, et al. (2003) Activation and regulation of Toll-like receptors 2 and 1 in human leprosy. Nat Med 9: 525–532.
9. Takeuchi O, Sato S, Horiuchi T, Hoshino K, Takeda K, et al. (2002) Cutting edge: role of Toll-like receptor 1 in mediating immune response to microbial lipoproteins. J Immunol 169: 10–14.
10. Inaba K, Inaba M, Naito M, Steinman RM (1993) Dendritic cell progenitors phagocytose particulates, including bacillus Calmette-Guerin organisms, and sensitize mice to mycobacterial antigens in vivo. J Exp Med 178: 479–488.
11. Makino M, Maeda Y, Mukai T, Kaufmann SH (2006) Impaired maturation and function of dendritic cells by mycobacteria through IL-1beta. Eur J Immunol 36: 1443–1452.
12. Flynn JL, Chan J, Triebold KJ, Dalton DK, Stewart TA, et al. (1993) An essential role for interferon gamma in resistance to *Mycobacterium tuberculosis* infection. J Exp Med 178: 2249–2254.
13. Stenger S, Modlin RL (2002) Control of *Mycobacterium tuberculosis* through mammalian Toll-like receptors. Curr Opin Immunol 14: 452–457.
14. Gansert JL, Kiessler V, Engele M, Wittke F, Rollinghoff M, et al. (2003) Human NKT cells express granulysin and exhibit antimycobacterial activity. J Immunol 170: 3154–3161.
15. Kaufmann SH (1999) Cell-mediated immunity: dealing a direct blow to pathogens. Curr Biol 9: R97–99.
16. Thoma-Uszynski S, Stenger S, Modlin RL (2000) CTL-mediated killing of intracellular *Mycobacterium tuberculosis* is independent of target cell nuclear apoptosis. J Immunol 165: 5773–5779.
17. Makino M, Baba M (1997) A cryopreservation method of human peripheral blood mononuclear cells for efficient production of dendritic cells. Scand J Immunol 45: 618–622.
18. Maeda Y, Mukai T, Spencer J, Makino M (2005) Identification of an immunomodulating agent from *Mycobacterium leprae*. Infect Immun 73: 2744–2750.
19. Levy L, Ji B (2006) The mouse foot-pad technique for cultivation of *Mycobacterium leprae*. Lepr Rev 77: 5–24.
20. McDermott-Lancaster RD, Ito T, Kohsaka K, Guelpa-Lauras CC, Grosset JH (1987) Multiplication of *Mycobacterium leprae* in the nude mouse, and some applications of nude mice to experimental leprosy. Int J Lepr Other Mycobact Dis 55: 889–895.
21. Hashimoto K, Maeda Y, Kimura H, Suzuki K, Masuda A, et al. (2002) *Mycobacterium leprae* infection in monocyte-derived dendritic cells and its influence on antigen-presenting function. Infect Immun 70: 5167–5176.
22. Hendry C, Dionne K, Hedgepeth A, Carroll K, Parrish N (2009) Evaluation of a rapid fluorescent staining method for detection of mycobacteria in clinical specimens. J Clin Microbiol 47: 1206–1208.
23. Truman RW, Krahenbuhl JL (2001) Viable *Mycobacterium leprae* as a research reagent. Int J Lepr Other Mycobact Dis 69: 1–12.
24. Kishida Y, Yoshikawa H, Myoui A (2007) Parthenolide, a natural inhibitor of Nuclear Factor-kappaB, inhibits lung colonization of murine osteosarcoma cells. Clin Cancer Res 13: 59–67.
25. Bastian M, Braun T, Bruns H, Rollinghoff M, Stenger S (2008) Mycobacterial lipopeptides elicit CD4+ CTLs in *Mycobacterium tuberculosis*-infected humans. J Immunol 180: 3436–3446.

26. Murray RA, Siddiqui MR, Mendillo M, Krahenbuhl J, Kaplan G (2007) *Mycobacterium leprae* inhibits dendritic cell activation and maturation. J Immunol 178: 338–344.
27. Cella M, Scheidegger D, Palmer-Lehmann K, Lane P, Lanzavecchia A, et al. (1996) Ligation of CD40 on dendritic cells triggers production of high levels of interleukin-12 and enhances T cell stimulatory capacity: T-T help via APC activation. J Exp Med 184: 747–752.
28. Yamauchi PS, Bleharski JR, Uyemura K, Kim J, Sieling PA, et al. (2000) A role for CD40-CD40 ligand interactions in the generation of type 1 cytokine responses in human leprosy. J Immunol 165: 1506–1512.
29. Sallusto F, Cella M, Danieli C, Lanzavecchia A (1995) Dendritic cells use macropinocytosis and the mannose receptor to concentrate macromolecules in the major histocompatibility complex class II compartment: downregulation by cytokines and bacterial products. J Exp Med 182: 389–400.
30. Tailleux L, Schwartz O, Herrmann JL, Pivert E, Jackson M, et al. (2003) DC-SIGN is the major *Mycobacterium tuberculosis* receptor on human dendritic cells. J Exp Med 197: 121–127.
31. Geijtenbeek TB, Van Vliet SJ, Koppel EA, Sanchez-Hernandez M, Vandenbroucke-Grauls CM, et al. (2003) Mycobacteria target DC-SIGN to suppress dendritic cell function. J Exp Med 197: 7–17.
32. Langrish CL, McKenzie BS, Wilson NJ, de Waal Malefyt R, Kastelein RA, et al. (2004) IL-12 and IL-23: master regulators of innate and adaptive immunity. Immunol Rev 202: 96–105.
33. Pearce EL, Shen H (2007) Generation of CD8 T cell memory is regulated by IL-12. J Immunol 179: 2074–2081.
34. Shibagaki N, Udey MC (2002) Dendritic cells transduced with protein antigens induce cytotoxic lymphocytes and elicit antitumor immunity. J Immunol 168: 2393–2401.
35. Brightbill HD, Libraty DH, Krutzik SR, Yang RB, Belisle JT, et al. (1999) Host defense mechanisms triggered by microbial lipoproteins through toll-like receptors. Science 285: 732–736.
36. Stenger S, Modlin RL (1999) T cell mediated immunity to *Mycobacterium tuberculosis*. Curr Opin Microbiol 2: 89–93.
37. van de Berg PJ, van Leeuwen EM, ten Berge IJ, van Lier R (2008) Cytotoxic human CD4(+) T cells. Curr Opin Immunol 20: 339–343.
38. Canaday DH, Wilkinson RJ, Li Q, Harding CV, Silver RF, et al. (2001) CD4(+) and CD8(+) T cells kill intracellular *Mycobacterium tuberculosis* by a perforin and Fas/Fas ligand-independent mechanism. J Immunol 167: 2734–2742.
39. Ochoa MT, Stenger S, Sieling PA, Thoma-Uszynski S, Sabet S, et al. (2001) T-cell release of granulysin contributes to host defense in leprosy. Nat Med 7: 174–179.
40. Dieli F, Troye-Blomberg M, Ivanyi J, Fournie JJ, Krensky AM, et al. (2001) Granulysin-dependent killing of intracellular and extracellular *Mycobacterium tuberculosis* by Vgamma9/Vdelta2 T lymphocytes. J Infect Dis 184: 1082–1085.
41. Heibein JA, Barry M, Motyka B, Bleackley RC (1999) Granzyme B-induced loss of mitochondrial inner membrane potential (Delta Psi m) and cytochrome c release are caspase independent. J Immunol 163: 4683–4693.
42. Davis JE, Smyth MJ, Trapani JA (2001) Granzyme A and B-deficient killer lymphocytes are defective in eliciting DNA fragmentation but retain potent in vivo anti-tumor capacity. Eur J Immunol 31: 39–47.

doi:10.1016/j.jmb.2011.04.059 J. Mol. Biol. (2011) 410, 93–104

Contents lists available at www.sciencedirect.com

Journal of Molecular Biology

journal homepage: http://ees.elsevier.com.jmb

Structural Insights into the Novel Diadenosine 5′,5‴-P^1,P^4-Tetraphosphate Phosphorylase from *Mycobacterium tuberculosis* H37Rv

Shigetarou Mori*, Keigo Shibayama, Jun-Ichi Wachino and Yoshichika Arakawa

Department of Bacteriology II, National Institute of Infectious Diseases, 4-7-1 Gakuen, Musashi-Murayama-shi, Tokyo 208-0011, Japan

Received 25 October 2010; received in revised form 22 April 2011; accepted 23 April 2011
Available online 4 May 2011

Edited by M. Guss

Keywords:
X-ray crystallography; mycobacteria; nucleotide; mutation; kinetics

Rv2613c is a diadenosine 5′,5‴-P^1,P^4-tetraphosphate (Ap_4A) phosphorylase from *Mycobacterium tuberculosis* H37Rv. Sequence analysis suggests that Rv2613c belongs to the histidine triad (HIT) motif superfamily, which includes HIT family diadenosine polyphosphate (Ap_nA) hydrolases and Ap_4A phosphorylases. However, the amino acid sequence of Rv2613c is more similar to that of HIT family Ap_nA hydrolases than to that of typical Ap_4A phosphorylases. Here, we report the crystal structure of Rv2613c, which is the first structure of a protein with Ap_nA phosphorylase activity, and characterized the structural basis of its catalytic activity. Our results showed that the structure of Rv2613c is similar to those of other HIT superfamily proteins. However, Asn139, Gly146, and Ser147 in the active site of Rv2613c replace the corresponding Gln, Gln, and Thr residues that are normally found in HIT family Ap_nA hydrolases. Furthermore, analyses of Rv2613c mutants revealed that Asn139, Gly146, and Ser147 are important active-site residues and that Asn139 has a critical role in catalysis. The position of Gly146 might influence the phosphorylase activity. In addition, the tetrameric structure of Rv2613c and the presence of Trp160 might be essential for the formation of the Ap_4A binding site. These structural insights into Rv2613c may facilitate the development of novel structure-based inhibitors for treating tuberculosis.

Introduction

Mycobacterium tuberculosis is the causative agent of tuberculosis (TB). Every year, approximately 1.7 million people die from TB worldwide, and more than 8.9 million people are newly infected with *M. tuberculosis*.[1] Furthermore, multidrug-resistant TB and extensively drug-resistant TB have become serious problems recently.[2] As a result, novel anti-TB drugs are needed urgently. To facilitate the structure-based design of new anti-TB drugs, our group has investigated the structure–function relationships of *M. tuberculosis* proteins such as the NAD kinase–NAD complex[3] and Rv2613c, which is a novel diadenosine 5′,5‴-P^1,P^4-tetraphosphate (Ap_4A) phosphorylase (EC 2.7.7.53).[4] The *Rv2613c* gene was previously shown to be an essential gene in *M. tuberculosis* H37Rv,[5] and Rv2613c was recognized as a target for new anti-TB drugs by *in silico* analysis.[6] Therefore, we have determined the

**Corresponding author*. E-mail address: mshige@nig.go.jp.

Abbreviations used: Ap_4A, diadenosine 5′,5‴-P^1,P^4-tetraphosphate; HIT, histidine triad; Ap_nA, diadenosine polyphosphate; TB, tuberculosis; SAD, single-wavelength anomalous dispersion; PDB, Protein Data Bank; AMW, adenosine monotungstate; IB2, P^1,P^2-methylene-P^3-thio-diadenosine triphosphate; SeMet, selenomethionine.

three-dimensional structure of Rv2613c and elucidated its structure–function relationships.

Since the amino acid sequence of Rv2613c has a histidine triad (HIT) motif (His-φ-His-φ-His-φ-φ, where φ represents a hydrophobic amino acid), Rv2613c is thought to belong to the HIT superfamily. This superfamily also includes nucleotide hydrolases and transferases such as adenosine monophosphate (AMP) lysine hydrolases, HIT family diadenosine polyphosphate (Ap_nA) hydrolases, galactose-1-phosphate uridylyltransferases, and Ap_4A phosphorylases.[7] The amino acid sequence of Rv2613c has both similarities with and differences from the sequences of other Ap_4A phosphorylases in the HIT superfamily. For example, *Kluyveromyces lactis* Ap_4A phosphorylase (Swiss-Prot ID: APA2_KLULA) and *Saccharomyces cerevisiae* Ap_4A phosphorylases 1 and 2 (Swiss-Prot IDs: APA1_YEAST and APA2_YEAST) have a His-X-His-X-Gln motif instead of the HIT motif.[8,9] In addition, unlike these phosphorylases, which are approximately 330 amino acids long,[8,9] Rv2613c is only 195 amino acids long; therefore, its length is similar to that of *Schizosaccharomyces pombe* Ap_nA hydrolase (Swiss-Prot ID: APH1_SCHPO), which is 182 amino acids long.[10] Furthermore, the amino acid sequence of Rv2613c is more similar to that of HIT family Ap_nA hydrolases than typical Ap_4A phosphorylases. For instance, the amino acid sequence of Rv2613c is 28.8% identical and 61.9% similar to *Sc. pombe* Ap_nA hydrolase, whereas it is 16.2% identical and 60.7% similar to *S. cerevisiae* Ap_4A phosphorylase 1. Collectively, these observations suggest that the amino acid sequence of Rv2613c is more related to HIT family Ap_nA hydrolases than to typical Ap_4A phosphorylases.

Furthermore, we recently showed that Rv2613c converts Ap_4A into ATP and adenosine 5′-diphosphate (ADP) in the presence of inorganic phosphate (Eq. (1)), so it is a phosphorylase rather than a hydrolase.[4] In contrast, HIT family Ap_nA hydrolases convert Ap_nA into Ap_{n-1} and AMP (Eq. (2)):[7]

$$Ap_4A + \text{inorganic phosphate} \rightarrow ATP + ADP \quad (1)$$

$$Ap_nA \rightarrow Ap_{n-1} + AMP \quad (2)$$

Previous crystallographic studies of HIT superfamily proteins have revealed that the HIT motif is part of the substrate binding site and that the conserved central His residue in the HIT motif is important for catalytic activity.[11,12] In addition, a Ser residue, which is upstream of the HIT motif, is important for the catalytic activity of AMP-lysine hydrolase[13] and galactose-1-phosphate uridylyltransferase.[14] However, the three-dimensional structure and catalytic residues of an Ap_4A phosphorylase are not known. Therefore, we aimed to determine the crystal structure of Rv2613c and to characterize and compare the structural basis of its catalytic activity with those of HIT family Ap_nA hydrolases and typical Ap_4A phosphorylases.

Previously, we also showed that the multimerization of Rv2613c differs from those of HIT family Ap_nA hydrolases and typical Ap_4A phosphorylases.[4] Specifically, Rv2613c is homotetrameric in solution,[4] whereas HIT family Ap_nA hydrolases and typical Ap_4A phosphorylases are homodimeric[15] and monomeric,[16,17] respectively. Therefore, we also investigated the importance of multimerization for the catalytic activity of Rv2613c.

Recently, we reported the crystallization and preliminary X-ray analysis of Rv2613c.[18] Here, we describe the 1.89-Å-resolution crystal structure of Rv2613c and provide insights into the structural basis of its catalytic activity. To our knowledge, this is the first report of the crystal structure of a protein with Ap_nA phosphorylase activity.

Results

Structure determination

Previously, we showed that the Rv2613c crystal belongs to the *C*2 space group and has unit cell parameters of $a=101.5$ Å, $b=63.6$ Å, $c=79.1$ Å, and $\beta=110.9°$.[18] In addition, we reported that Rv2613c exists as a homotetramer of 25-kDa subunits in solution[4] and that there are two subunits per asymmetric unit, which are characterized by a V_m of 2.41 $Å^3$ Da^{-1} and a solvent content of 49.1%.[18] Here, we solved the crystal structure of Rv2613c at 1.89 Å resolution by using single-wavelength anomalous dispersion (SAD). The final *R*-factor and R_{free} were 17.6% and 20.1%, respectively (Table 1). The final model of Rv2613c consisted of 325 residues, 233 water molecules, 3 phosphate ions, and 2 tetraethylene glycols in the asymmetric unit, which included subunits A and B (Rv2613c-A/-B) (Fig. 1a). Electron density was present for all residues in Rv2613c-A, except for the His tag and for residues 1–13, 36–54, and 171–175. Similarly, electron density was present for all residues in Rv2613c-B, except for the His tag and for residues 1–23. In addition, residues 196–198 in Rv2613c-B were derived from the expression vector. The average *B*-factors for all atoms of Rv2613c-A, Rv2613c-B, water molecules, phosphate ions, and tetraethylene glycols were 32.7, 26.5, 36.3, 36.6, and 43.8 $Å^2$, respectively. Ramachandran plot analysis showed that the φ/ψ angle pairs of most residues (322/325; 99.1%) were in the favored regions, whereas the pairs of the remaining residues (3/325; 0.9%) were in the allowed regions (Table 1).

Table 1. Data collection and structure refinement statistics

	Native	SeMet
Data collection		
Wavelength (Å)	1.00000	0.97901
Resolution range (Å)	50.0–1.89 (1.93–1.89)[a]	50.0–2.50 (2.54–2.50)
Space group	*C*2	*C*2
Cell dimensions *a*, *b*, *c* (Å)	101.5, 63.6, 79.1	101.3, 63.5, 79.5
Cell dimension β (°)	110.9	110.6
Unique reflections	37,314 (1826)	16,529 (808)
Average redundancy	7.4 (6.4)	7.6 (7.3)
Completeness (%)	99.8 (98.3)	99.9 (99.9)
Mean $I/\sigma(I)$	42.2 (4.4)	33.6 (6.9)
R_{merge}[b]	6.1 (38.0)	8.6 (33.4)
Refinement		
Resolution range	39.4–1.89 (1.94–1.89)	
Number of reflections	36,096 (2327)	
R-factor (%)[c]	17.6 (19.5)	
R_{free} (%)[d]	20.1 (26.6)	
RMSD from ideality		
Bonds (Å)	0.005	
Angles (°)	1.025	
Ramachandran plot		
Favored region (%)	99.1	
Allowed region (%)	0.9	
Outlier region (%)	0	

[a] Data for the highest-resolution shells are given in parentheses.
[b] $R_{merge} = \sum_{hkl}\sum_i |I_i(hkl) - \langle I(hkl)\rangle| / \sum_{hkl}\sum_i I_i(hkl)$, where $I_i(hkl)$ is the *i*th intensity measurement of reflection *hkl* and $\langle I(hkl)\rangle$ is its average.
[c] *R*-factor $= \sum_{hkl}|F_{obs} - k|F_{calc}| / \sum_{hkl}|F_{obs}|$, where *k* is the scaling factor.
[d] This value is based on 5% of the data excluded from refinement at random.

Protein architecture and conformation of prosthetic groups

The overall structure of Rv2613c consisted of a small N-terminal domain (residues 1–39) and a large C-terminal domain (residues 40–195). In Rv2613c-A, the N-terminal domain consisted of two β-strands, whereas in Rv2613c-B, the N-terminal domain consisted of one α-helix and one β-strand (Fig. 1a and b). The C-terminal domain formed an α/β structure in both Rv2613c-A and Rv2613c-B, and was involved in the dimer interaction between Rv2613c-A and Rv2613c-B in the asymmetric unit (Fig. 1a and b). The main structural feature of this dimer was an antiparallel β-sheet with a normal left-handed twist (Fig. 1a). This β-sheet consisted of 10 β-strands, which included strands C, D, E, G, and F from Rv2613c-A, and strands M, N, L, K, and J from Rv2613c-B (Fig. 1a and b). Two long α-helices (α4 in Rv2613c-A and α12 in Rv2613c-B) also were involved in the dimer interaction and were located inside this β-sheet (Fig. 1a and b).

The quaternary structure of Rv2613c was a tetramer consisting of a dimer of dimers (Rv2613c-A/-B+Rv2613c-A′/-B′) (Fig. 1c), in agreement with our previous observation that Rv2613 tetramerizes in solution.[4] The N-terminal domain was involved in intersubunit contacts (Fig. 1b and c). Specifically, at the A–B′ contact, a mixed β-sheet and a parallel β-sheet consisted of three β-strands (A and H from Rv2613c-A and I′ from Rv2613c-B′) and two β-strands (B from Rv2613c-A and O′ from Rv2613c-B′). Similarly, at the B–A′ contact, a mixed β-sheet and a parallel β-sheet also were composed of three β-strands (I from Rv2613c-B, and A′ and H′ from Rv2613c-A′) and two β-strands (O from Rv2613c-B and B′ from Rv2613c-A′) (Fig. 1b and c). In addition, three α-helices (α6 in Rv2613c-A, and α8 and α15 in Rv2613c-B) were involved in this tetramerization (Fig. 1c).

In Rv2613c-A, one phosphate ion and one tetraethylene glycol were bound to the C-terminal domain, while two phosphate ions and one tetraethylene glycol were bound to the C-terminal domain in Rv2613c-B (Fig. 1a). One phosphate ion was bound to the same binding site in each subunit, while the other phosphate ion in Rv2613c-B was bound to the C-terminal domain (Fig. 1a). In addition, the binding site and conformation of tetraethylene glycol molecule in Rv2613c-A were different from those of the tetraethylene glycol molecule in Rv2613c-B (Fig. 1a).

Structural comparisons

We searched for similar protein structures. As a result, the structure of Rv2613c is similar to those of other proteins in the HIT superfamily such as *Homo sapiens* fragile HIT protein [Fhit; Protein Data Bank (PDB) IDs: 6FIT and 1FHI; Z-score=16.1 and 15.8, respectively], which is a HIT family Ap_nA hydrolase;[11,12] Zn-bound HIT family protein from *Mycobacterium smegmatis* (MSMEG5028; PDB ID: 3O0M; Z-score=16.1); and ADP-glucose phosphorylase from *Arabidopsis thaliana* (Ath; PDB ID: 1Z84; Z-score=11.5).[19] For example, superimposition of the structures of Rv2613c, Fhit, and MSMEG5028 revealed that the structure of Rv2613c-A/-B is similar to those of the Fhit and MSMEG5028 dimers (Fig. 2a). In particular, the 10-stranded antiparallel β-sheet and inner long α-helices of the Rv2613c dimer were in good agreement with those of the Fhit and MSMEG5028 dimers (Fig. 2a). In contrast, neither Fhit nor MSMEG5028 was structurally similar to the N-terminal domain of Rv2613c (Fig. 2a).

In addition, since this is the first report of the crystal structure of a protein with Ap_nA phosphorylase activity, we compared the structure of Rv2613c with that of Ath in place of a typical Ap_4A phosphorylase. Ath has a His-X-His-X-Gln motif, which is characteristic of typical Ap_4A phosphorylases. In addition, the amino acid sequence of Ath is 36% identical and 56% similar to *S. cerevisiae* Ap_4A phosphorylase 1. Therefore, we considered the

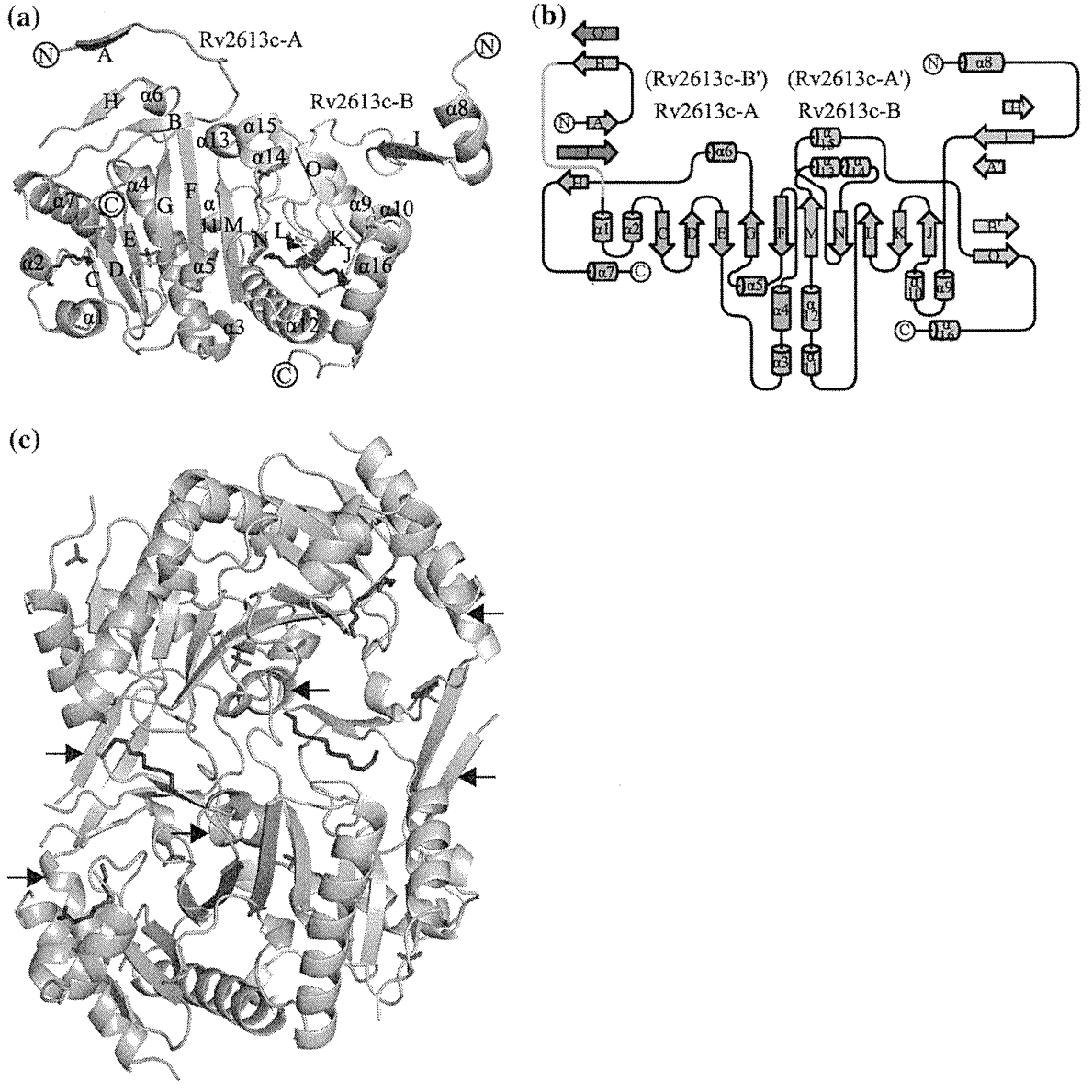

Fig. 1. Structure of Rv2613c. (a) Ribbon diagram of Rv2613c subunit A (green) and subunit B (cyan) (Rv2613c-A/-B) in the asymmetric unit. The N-terminus and the C-terminus are indicated by circled letters. α-Helices are numbered, and β-strands are lettered in order from the N-terminus of Rv2613c-A to the C-terminus of Rv2613c-B. Phosphate ions and tetraethylene glycols are modeled as red and blue sticks, respectively. (b) Secondary structure of the Rv2613c dimer shown in (a). Rv2613c-A and Rv2613c-B are indicated in green and cyan, respectively. The N-terminus, C-terminus, α-helices, and β-strands are labeled as in (a). In Rv2613c-A, the loops, which were not modeled due to poor electron density, are shown as gray lines. The three β-strands from Rv2613c-A′ and the two β-strands from Rv2613c-B′ are shown in yellow and red, respectively. (c) Ribbon diagram of the quaternary structure of Rv2613c. The asymmetric unit contains two subunits (Rv2613c-A/-B or Rv2613c-A′/-B′). Rv2613c-A, Rv2613c-B, Rv2613c-A′, and Rv2613c-B′ are shown in green, cyan, yellow, and light brown, respectively. Phosphate ions and tetraethylene glycols are represented as in (a). The arrows show A–B′ and B–A′ contacts.

structure of Ath an appropriate comparison structure. Superimposition of the structures of Rv2613c and Ath showed that the structure of Rv2613c-A/-B is similar to that of the Ath monomer (Fig. 2b). In particular, the 10-stranded antiparallel β-sheet and inner long α-helices of the Rv2613c dimer were in good agreement with that of the Ath monomer (Fig. 2b). In addition, Ath exhibited structural similarity to the N-terminal domain of Rv2613c (Fig. 2b). Furthermore, the structure of the Rv2613c tetramer was similar to that of the Ath dimer. Moreover, the interaction between Rv2613c-A/-B and Rv2613c-A′/-B′ also was similar to the interaction in the Ath dimer. Finally, unlike the crystal

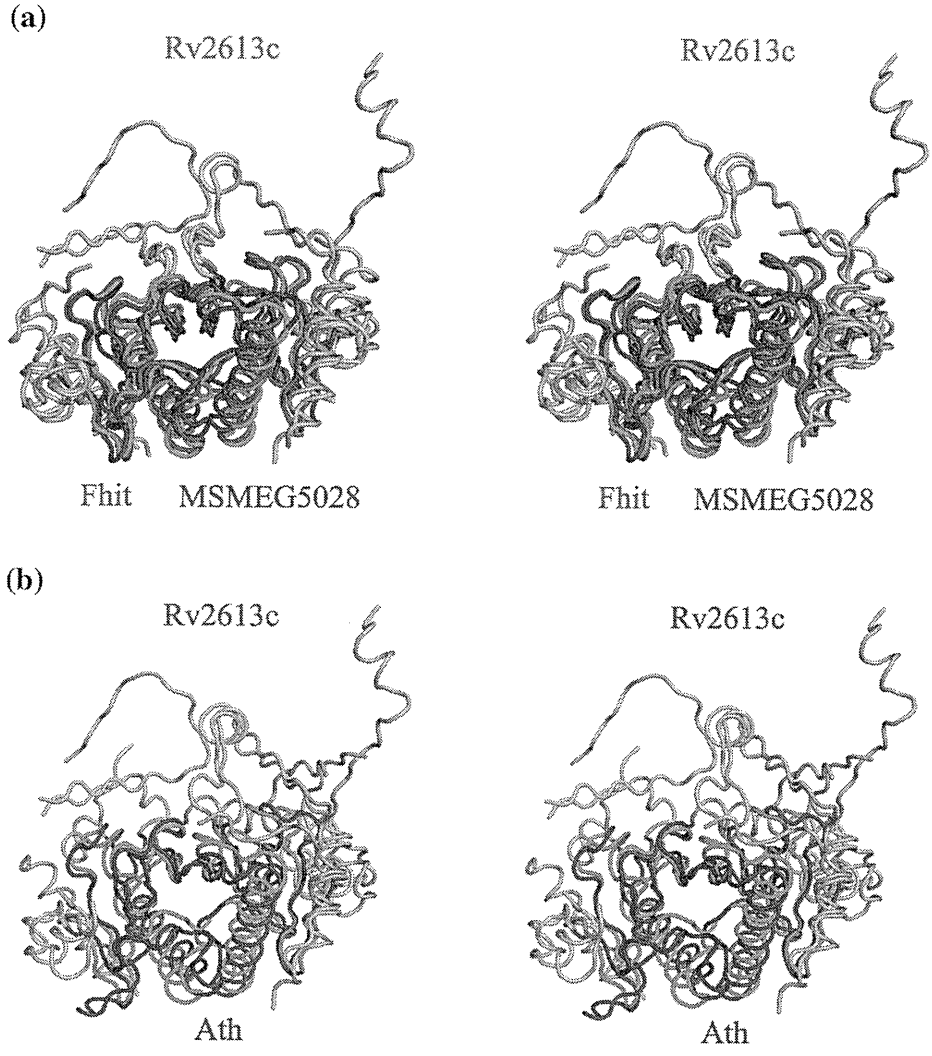

Fig. 2. Stereo representation of structural comparisons between Rv2613c and representative proteins in the HIT superfamily. (a) Superimposition of the structure of Rv2613c-A/-B on those of *H. sapiens* Fhit (PDB ID: 6FIT) and the Zn-bound HIT family protein from *M. smegmatis* (MSMEG5028; PDB ID: 3O0M) dimers. Rv2613c, Fhit, and MSMEG5028 are shown in green, red, and blue, respectively. Regions that are structurally similar are illustrated with darker colors compared to those that are divergent. (b) Superimposition of the structure of Rv2613c-A/-B on that of the ADP-glucose phosphorylase from *A. thaliana* (Ath; PDB ID: 1Z84) monomer. Rv2613c and Ath are shown in green and blue, respectively. Regions that are structurally similar are depicted with darker colors compared to those that are divergent. The structurally similar region of the Ath monomer is probably an internally duplicated subdomain.

structures of MSMEG5028 and Ath, which include a zinc ion, the crystal structures of Rv2613c and Fhit did not include any metal ions.

Catalytically important residues

The binding site of the phosphate ion in Rv2613c (Fig. 3a) corresponded to that of the tungstate ion of adenosine monotungstate (AMW) in Fhit (Fig. 3b) and that of the α-phosphate of AMP in Ath (Fig. 3c). Since HIT superfamily proteins, including Rv2613c, act on the α-phosphate of ribonucleotides,[4,7] it is likely that the phosphate ion binding site of Rv2613c is its active site. In this site, Asn139, Ser147, His153, and His155 were bound to the phosphate ion, and Gly146 was positioned near the phosphate ion (Fig. 3a). Thus, these five residues are probably catalytically important for the enzyme activity of Rv2613c.

Furthermore, the multiple sequence alignment of Rv2613c and related HIT superfamily proteins provides additional evidence for the importance of these residues. For example, His153 and His155 were in the HIT motif, whereas Asn139, Gly146, and Ser147 were upstream of this motif (Fig. 4). In addition, the multiple sequence alignment of the region containing these five residues in the

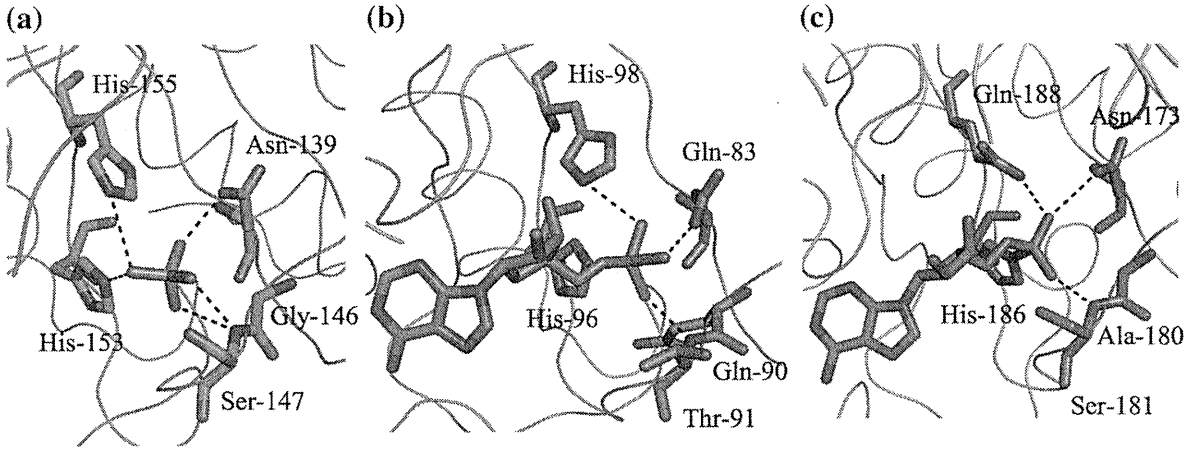

Fig. 3. Comparison of the active sites of Rv2613c, Fhit, and Ath. (a) Active site of Rv2613c. Asn139, Gly146, Ser147, His153, His155, and the phosphate ion are represented by sticks. Carbon, nitrogen, oxygen, and phosphorus atoms are shown in green, blue, red, and orange, respectively. (b) Active site of Fhit (PDB ID: 6FIT). Gln83, Gln90, Thr91, His96, His98, and AMW are represented by sticks. The carbon atoms in the amino acids and adenosine are shown in orange and purple, respectively. Nitrogen, oxygen, and tungsten atoms are shown in blue, red, and cyan, respectively. (c) Active site of Ath (PDB ID: 1Z84). Asn173, Ala180, Ser181, His186, Gln188, and AMP are represented by sticks. The carbon atoms in the amino acids and adenosine are shown in light blue and purple, respectively. Nitrogen, oxygen, and phosphorus atoms are shown in dark blue, red, and orange, respectively.

phosphate binding site of Rv2613c and the corresponding residues in the AMW binding site of Fhit showed that His153 and His155 in Rv2613c correspond to His96 and His98 in Fhit, respectively (Figs. 3a and b and 4). Similarly, Asn139, Gly146, and Ser147 in Rv2613c are equivalent to Gln83, Gln90, and Thr91 in Fhit, respectively (Figs. 3a and b and 4). In addition, the Gln, Gln, and Thr residues, which corresponded to Gln83, Gln90, and Thr91, respectively, in Fhit were conserved among HIT family Ap_nA hydrolases (Fig. 4). On the other hand, the multiple sequence alignment showed that Asn139, Ser147, and His153 in the phosphate binding site of Rv2613c corresponded to Asn173, Ser181, and His186 in the AMP binding site of Ath, respectively (Figs. 3a and c and 4). Similarly, Gly146 and His155 in Rv2613c are equivalent to Ala180 and Gln188 in Ath, respectively (Figs. 3a and c and 4). In addition, the Asn and Ser residues, which corresponded to Asn139 and Ser147, respectively, in Rv2613c were conserved among Ap_4A phosphorylases and ADP-glucose phosphorylase (Fig. 4).

```
                          146       153
                  139     147       155     160
Rv2613c           GLNLGTSAGGSLAEHLHVHVVPRWGGDANFI
APA2_KLULA        FYNCGPNSGSSQ-DHKHLQILPLPYKFVPYQ
APA1_YEAST        FYNSGPASGSSL-DHKHLQILQMPEKFVTFQ
APA2_YEAST        FYNCGPHSGSSQ-DHKHLQIMQMPEKFIPFQ
Fhit              SMQDGPEAGQTV-KHVHVHVLPRKAGDFHRN
FHIT_MOUSE        SMQDGPEAGQTV-KHVHVHVLPRKAGDFPRN
APH1_SCHPO        GIQDGVDAGQTV-PHVHVHIIPRKKADFSEN
Ath               FKNQGASAGASM-SHSHSQMMALPVVPPTVS
                    : *   :*      * * :::
```

Fig. 4. Multiple sequence alignment of the active-site region of Rv2613c and representative Ap_4A phosphorylases (APA2_KLULA, APA1_YEAST, and APA2_YEAST) and HIT family Ap_nA hydrolases [Fhit; FHIT_MOUSE (*Mus musculus*); and APH1_SCHPO], and ADP-glucose phosphorylase (Ath). The Swiss-Prot (UniProtKB) IDs of these proteins are as follows: Rv2613c (O06201), APA2_KLULA (P49348), APA1_YEAST (P16550), APA2_YEAST (P22108), Fhit (P49789), FHIT_MOUSE (O89106), APH1_SCHPO (P49776), and Ath (Q9FK51). The position of residues in Rv2613c is shown above the alignment. The residues that correspond to Asn139, Gly146, Ser147, His153, and His155 in Rv2613c are highlighted in blue, while those that correspond to Trp160 in Rv2613c are highlighted in red. The HIT and His-X-His-X-Gln motifs are boxed. Identical and highly conserved residues are denoted by an asterisk (*) or a colon (:), respectively. The multiple sequence alignment was generated by CLUSTAL W 1.83.

Table 2. Kinetic values of Rv2613c and derivatives

Enzyme	Activity (U mg^{-1})[a]	K_m (mM)	K_{cat} (s^{-1})	K_{cat}/K_m (M^{-1} s^{-1})
Wild type	8.69	0.10±0.001	8.48±0.313	84.82
N139A	ND[b]	—	—	—
N139Q	ND	—	—	—
G146S	2.63	0.08±0.014	1.99±0.115	24.88
G146Q	1.19	0.08±0.019	1.38±0.108	17.25
S147A	0.96	0.07±0.015	0.48±0.036	6.90
S147T	1.92	0.11±0.018	1.49±0.130	13.62
N139Q/S147T	ND	—	—	—
W160A	ND	—	—	—

[a] Specific activity determined in the presence of 1.0 mM Ap_4A.
[b] ND, not detected (i.e., enzyme activity was not detected using up to 100 μg of purified enzyme for up to 2 h).

To test the hypothesis that Asn139, Ser147, and Gly146 are catalytically important residues in Rv2613c, we examined the catalytic activities of seven Rv2613c mutants, namely N139A, N139Q, G146S, G146Q, S147A, S147T, and N139Q/S147T. Three mutants (N139A, N139Q, and N139Q/S147T) did not exhibit any detectable catalytic activity, while the activity of the other four mutants (G146S, G146Q, S147A, and S147T) was lower than that of wild-type Rv2613c (Table 2). In addition, the K_m value of the G146S, G146Q, S147A, and S147T mutants was similar to that of wild-type Rv2613c; however, the K_{cat} and K_{cat}/K_m values of these four mutants were markedly lower than those of wild-type Rv2613c (Table 2).

We also determined the importance of Gly146 on the production of AMP during catalysis. Wild-type Rv2613c and G146S produced very little AMP (1.2 and 1.5 nmol from 100 nmol of Ap_4A, respectively; Fig. 5a and b), whereas G146Q produced more AMP (11.2 nmol from 100 nmol of Ap_4A; Fig. 5c).

Relationship between tetramerization and catalytic activity

To elucidate the relationship between the tetramerization and the catalytic activity of Rv2613c, we predicted the binding site of Ap_4A and its mode of binding in Rv2613c by superimposing the α-phosphate of Ap_4A on the phosphate ion in the putative active site of Rv2613c-A. As a result, one adenosine binding site corresponded to the tetraethylene glycol binding site in Rv2613c-A, while the other adenosine binding site corresponded to the tetraethylene glycol binding site in Rv2613c-B′ (Fig. 6a and b). Furthermore, the putative position of adenine, which was bound to Rv2613c-B′, could make π–π stacking interactions with Trp160 in this subunit (Fig. 6b). Therefore, we predicted that the tetramerization of Rv2613c (i.e., A–B′ and B–A′ contacts) is involved in the formation of the Ap_4A binding site and that Trp160 might participate in

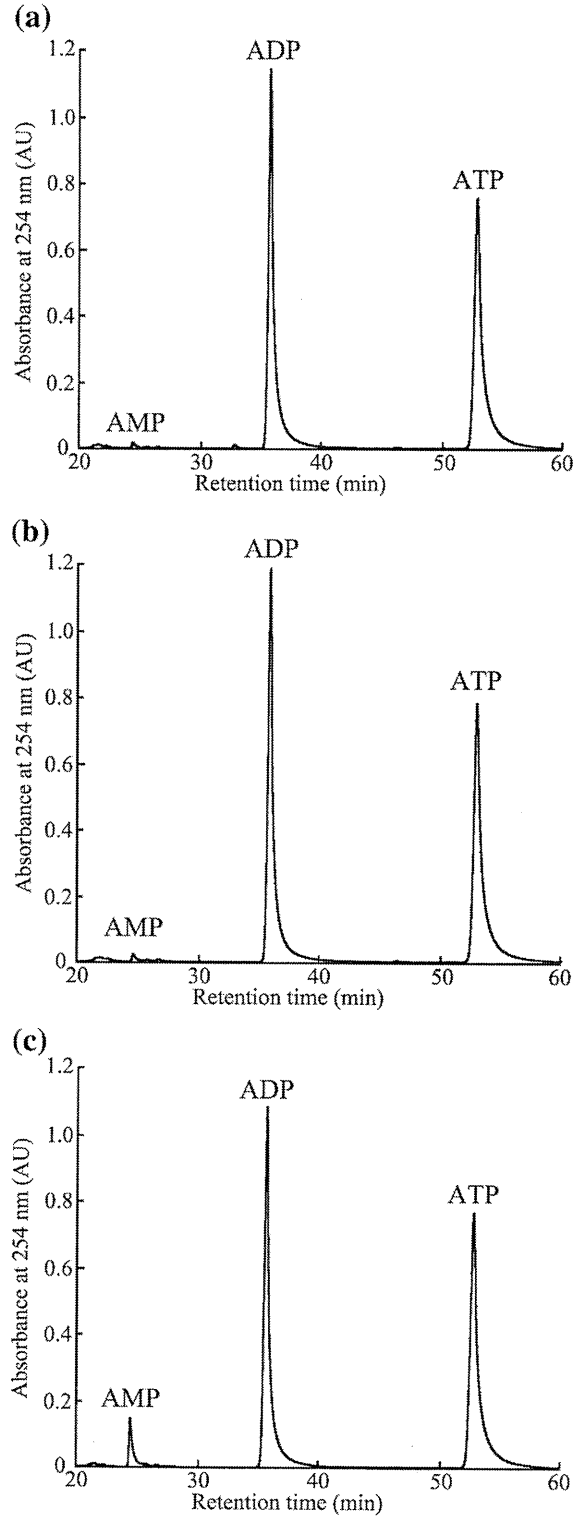

Fig. 5. High-performance liquid chromatography analyses of products formed by the complete degradation of 100 nmol of Ap_4A with purified Rv2613c (a), G146S (b), or G146Q (c). The reaction conditions are described in Materials and Methods.

the binding of Ap_4A. The latter hypothesis is supported by the observation that the W160A mutant of Rv2613c did not have any detectable catalytic activity (Table 2). In addition, the multiple sequence alignment in Fig. 4 showed that Trp160 in Rv2613c corresponds to a Pro residue in typical Ap_4A phosphorylases and ADP-glucose phosphorylase, and to a Lys residue in HIT family Ap_nA hydrolases. Finally, in the putative Ap_4A binding site of Rv2613c-A, the side

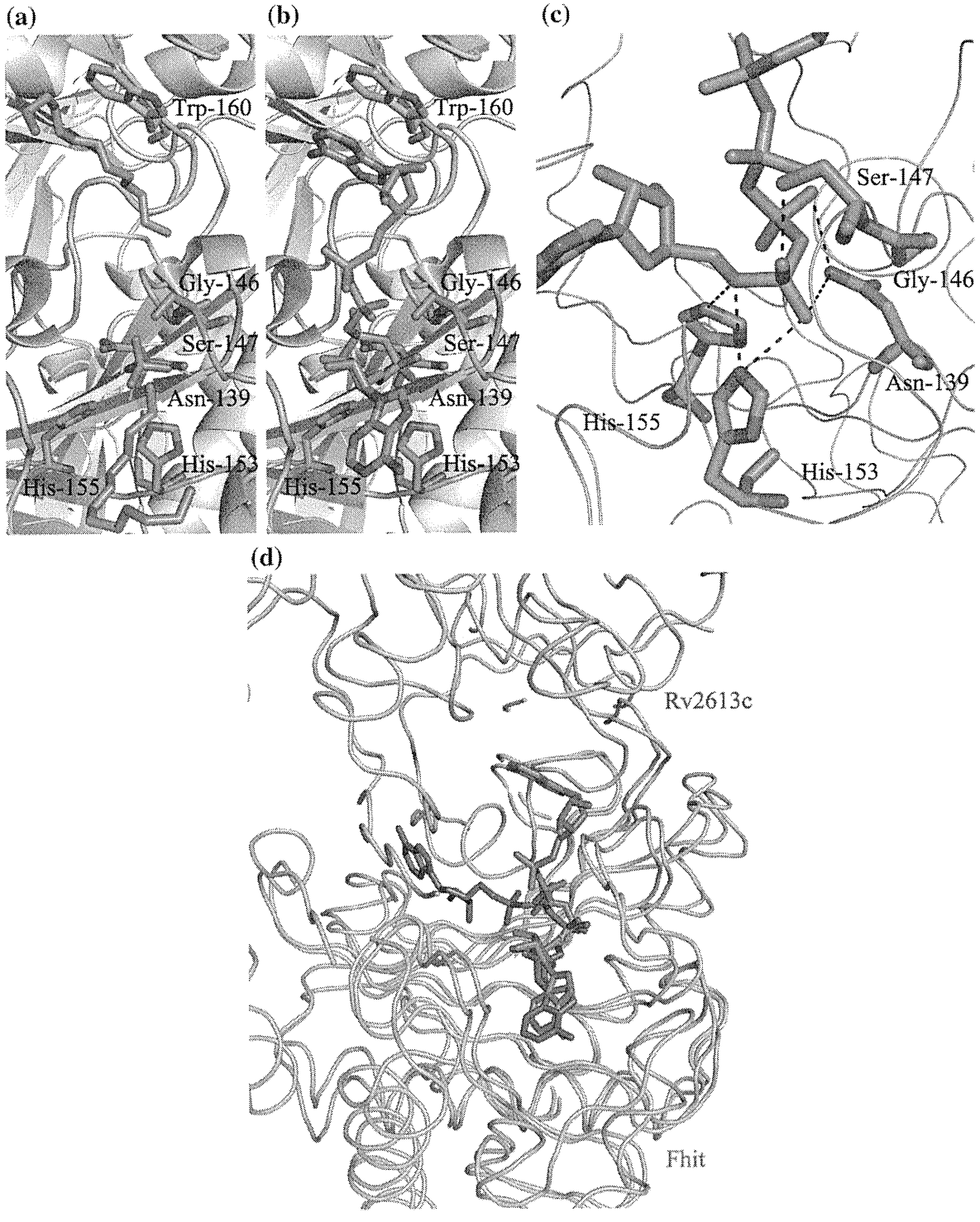

Fig. 6 *(legend on next page)*

chain of Asn139 would bind to both α-phosphoryl and β-phosphoryl oxygens of Ap_4A, and the side chains of Ser147, His153, and His155 would bind to the α-phosphoryl oxygen of Ap_4A (Fig. 6c).

A comparison of the putative Ap_4A binding site in Rv2613c with the P^1,P^2-methylene-P^3-thio-diadenosine triphosphate (IB2) binding site in Fhit[12] revealed that the putative binding site of the adenosine of Ap_4A in Rv2613c-A was the same as the adenosine binding site of IB2 in Fhit. However, the putative binding site of the other adenosine of Ap_4A in Rv2613c-B′ was different from the binding site of the other adenosine of IB2 in Fhit (Fig. 6d).

Discussion

Recently, we reported that Rv2613c is a tetrameric Ap_4A phosphorylase, but its amino acid sequence is more similar to HIT family Ap_nA hydrolases than to typical Ap_4A phosphorylases.[4] Now, we have solved the 1. 89-Å-resolution crystal structure of Rv2613c (Fig. 1a and Table 1), which is the first known structure of a protein with Ap_nA phosphorylase activity, and characterized the structural basis of its catalytic activity.

We found that the overall and active-site structures of Rv2613c were similar to those of other proteins in the HIT superfamily (Figs. 2 and 3). Specifically, the structure of Rv2613c-A/-B was in agreement with those of the Fhit dimer, MSMEG5028 dimer, and Ath monomer (Fig. 2a and b). Furthermore, a 10-stranded antiparallel β-sheet and long inner α-helices were common secondary structures in these proteins (Fig. 2a and b). Consistent with our previous results,[4] we also found that Rv2613c is tetrameric (Fig. 1c) and that its N-terminal domain is involved in intersubunit contacts (Fig. 1b and c). In contrast, Fhit and MSMEG5028 do not have a structural equivalent of the N-terminal domain of Rv2613c; therefore, they are homodimeric rather than tetrameric. In contrast, since Ath has a structural equivalent of the N-terminal domain of Rv2613c (Fig. 2b), it forms a homodimer, which corresponds to the Rv2613c tetramer. Therefore, a consensus structure of the N-terminal domain of Rv2613c might be required for the multimerization of HIT superfamily proteins.

In Rv2613c, one phosphate ion was bound to the same binding site in each subunit (Figs. 1c and 3a), which is thought to be the active site of Rv2613c. The interaction of Asn139 and Ser147 with the phosphate ion and the close proximity of Gly146 to the phosphate ion (Fig. 3a) suggested that these residues are catalytically important. We evaluated the catalytic importance of these residues by measuring the enzymatic activities of mutant Rv2613c proteins with point mutations in these residues. The lack of catalytic activity in the N139A, N139Q, and N139Q/S147T mutants (Table 2) showed that Asn139 is catalytically important. In addition, the similar K_m values and decreased K_{cat} values of the G146S, G146Q, S147A, and S147T mutants compared with those of wild-type Rv2613c (Table 2) suggested that Gly146 and Ser147 are probably important for the catalytic activity of Rv2613c rather than for Ap_4A binding. In the putative Ap_4A binding site of Rv2613c, the interactions between the side chain of Asn139 and the α-phosphoryl and β-phosphoryl oxygens of Ap_4A, as well as those between the side chain of Ser147 and the α-phosphoryl oxygen of Ap_4A (Fig. 6c), suggested that Asn139 and Ser147 are important to properly orient the α-phosphates and β-phosphates of Ap_4A for catalysis. This hypothesis is in agreement with two previous studies of HIT superfamily proteins, namely AMP-lysine hydrolase[13] and galactose-1-phosphate uridylyltransferase,[14] which showed the importance of a Ser residue in the active site. Furthermore, the catalytic importance of Asn139 and Ser147 in Rv2613c is consistent with the conservation of Asn and Ser residues at these positions in typical Ap_4A phosphorylases and ADP-glucose phosphorylase, but not in HIT family Ap_nA hydrolases, which have Gln and Thr residues in their active site (Figs. 3b and 4).

Fig. 6. Putative Ap_4A binding site in Rv2613c and comparison with the IB2 binding site in Fhit. (a) The binding sites for phosphate and tetraethylene glycol at the A–B′ contact of Rv2613c. Rv2613c subunits are colored as in Fig. 1c. Nitrogen, oxygen, and phosphorus atoms are shown in dark blue, red, and orange, respectively. The carbon atoms of tetraethylene glycol are shown in light blue. The carbon atoms of Asn139, Gly146, Ser147, His153, and His155 in Rv2613c-A are shown in green, and those of Trp160 in Rv2613c-B′ are shown in pink. (b) Putative Ap_4A binding site of Rv2613c. To create this model, we superimposed the α-phosphate of Ap_4A onto the phosphate ion in Rv2613c-A as shown in (a), and then we optimized the structure of Ap_4A by using the CNSsolve program. The Rv2613c subunits are colored as in Fig. 1c. The carbon atoms of adenosine are shown in light blue. Nitrogen, oxygen, and phosphorus atoms are colored as in (a). The carbon atoms of Asn139, Gly146, Ser147, His153, and His155 in Rv2613c-A, and those of Trp160 in Rv2613c-B′, are also colored as in (a). (c) Close-up view of the putative active sites of Rv2613c. Asn139, Gly146, Ser147, His153, His155, and Ap_4A colored as in (b). (d) Comparison of the putative binding mode of Ap_4A in Rv2613c and the binding mode of IB2 in Fhit (PDB ID: 1FHI). The backbones of the Rv2613c tetramer and the Fhit dimer are shown in green and light brown, respectively. Ap_4A and IB2 are shown in red and blue, respectively.

In addition to the catalytic importance of Gly146, the proximity of this residue to the α-phosphates and β-phosphates of Ap_4A in the putative Ap_4A binding site of Rv2613c (Fig. 6c) showed that this residue might influence the phosphorylase activity of Rv2613c. Moreover, G146Q produced about 10-fold more AMP than wild-type Rv2613c or G146S (Fig. 5). In addition, Gly146 in Rv2613c corresponds to Ser and Glu residues in typical Ap_4A phosphorylases and HIT family Ap_nA hydrolases, respectively (Fig. 4).

The structure of the predicted Ap_4A binding site of Rv2613c (Fig. 6b) and the lack of catalytic activity of the W160A mutant (Table 2) suggested that the tetramerization of Rv2613c (i.e., A–B′ and B–A′ contacts) and Trp160 may be essential for the formation of the Ap_4A binding site. Furthermore, the ability of Rv2613c to tetramerize, in contrast to the inability of Fhit to multimerize, might account for the difference between the putative Ap_4A binding site of Rv2613c and the IB2 binding site of Fhit (Fig. 6d).

The tetrameric structure of Rv2613c is unique among enzymes that use Ap_nA as a substrate. In addition, Trp160 in Rv2613c is not conserved in other Ap_4A phosphorylases and Ap_nA hydrolases in the HIT superfamily (Fig. 4). These differences suggest that Rv2613c may have a unique Ap_4A binding site, which may facilitate the design of specific inhibitors against Rv2613c. Ap_4A is found in both prokaryotes and eukaryotes,[20,21] and is involved in virulence and biofilm formation.[22,23] Furthermore, *Rv2613c* is an essential gene in *M. tuberculosis* H37Rv.[5] Therefore, the specific inhibitors against Rv2613c be potentially useful anti-TB drugs. As a result, we are currently screening for novel inhibitors of Rv2613c.

Materials and Methods

Selenomethionine substitution and site-directed mutagenesis of Rv2613c

The *Rv2613c* gene from *M. tuberculosis* H37Rv was cloned into the pCold I expression vector (Takara Bio, Inc., Shiga, Japan) to construct the pMS2613c plasmid, as described previously.[4] To express selenomethionine (SeMet)-substituted Rv2613c (SeMet-Rv2613c), we transformed pMS2613c into *Escherichia coli* B834(DE3) (Merck Novagen, Darmstadt, Germany). In addition, site-directed mutagenesis was used to introduce point mutations (N139A, N139Q, G146S, G146Q, S147A, S147T, N139Q/S147T, and W160A) into Rv2613 by using the QuickChange Site-Directed Mutagenesis Kit II (Agilent Technologies, Inc., Santa Clara, CA) with pMS2613c as template. The resulting plasmids were sequenced with an Applied Biosystems 3130*xl* Genetic Analyzer (Applied Biosystems, Carlsbad, CA) to confirm the mutation and were transformed into *E. coli* BL21(DE3)pLysS (Merck Novagen).

Expression and purification of Rv2613c

A single transformed colony of *E. coli* B834(DE3) was inoculated in 5 mL of Luria–Bertani medium and incubated overnight at 37 °C. Subsequently, 2 mL of the overnight culture was transformed into 200 mL of M9 minimal medium supplemented with the following: 1% glucose; 2 mM $MgSO_4$; 0.1 mM $CaCl_2$; 50 mg L^{-1} ampicillin; Kao Vitamins (Sigma-Aldrich Japan, Tokyo, Japan); 5 μg mL^{-1} each of L-Trp and L-Tyr; and 50 μg mL^{-1} each of L-Ala, L-Arg, L-Asn, L-Asp, L-Cys, L-Glu, L-Gln, L-Gly, L-His, L-Ile, L-Leu, L-Lys, L-Phe, L-Pro, L-Ser, L-Thr, L-Val, and L-SeMet. Then, this culture was grown under aerobic conditions for 7 h at 37 °C until the absorbance at 600 nm (A_{600}) had reached 1.0. Afterwards, the culture was transferred into 2 L of the same supplemented medium and cultured under the same conditions until an A_{600} of 0.4 had been reached. At that time, we added 0.5 mM isopropyl β-D-thiogalactopyranoside (Wako Pure Chemical Industries Ltd., Osaka, Japan) (final concentration) to induce protein expression and continued incubating the culture for 24 h at 15 °C. The Rv2613c point mutants were expressed in the same manner.

To purify the SeMet-Rv2613c and mutant Rv2613c proteins, we centrifuged the resulting *E. coli* cells at 8000*g* for 10 min at 4 °C, and then resuspended them in buffer A [20 mM sodium phosphate (pH 7.4), 0.5 M NaCl, and 40 mM imidazole]. Subsequently, the cells were disrupted by sonicating them on ice with a UP50H sonicator (Hielscher Ultrasonics, Teltow, Germany). Unbroken cells and cellular debris were removed by centrifugation at 20,000*g* for 30 min at 4 °C. Then, the clarified supernatant was loaded onto a HisTrap HP column (1.6 cm × 2.5 cm; GE Healthcare Bio-Sciences, Buckinghamshire, UK) that was equilibrated with buffer A, and the protein of interest was eluted with a linear gradient of imidazole (40–250 mM). Next, the protein was loaded onto a HiPrep 16/60 Sephacryl S-200 HR column (1.6 cm × 60 cm; GE Healthcare Bio-Sciences) that was equilibrated with buffer B [20 mM sodium phosphate (pH 7.4), 0.5 M NaCl, and 150 mM imidazole]. The sample was separated with buffer B into 1.2-mL fractions. For SeMet-Rv2613c, fractions 24–30 were pooled and then dialyzed against buffer C [20 mM 4-(2-hydroxyethyl)-1-piperazineethanesulfonic acid (Hepes)-Na (pH 7.6) and 0.5 mM dithiothreitol] using Slide-A-Lyzer Dialysis Cassettes (10,000 weight cutoff; Thermo Fisher Scientific, Waltham, MA) at room temperature. For the Rv2613c mutants, fraction 25 was dialyzed against buffer C using Slide-A-Lyzer Dialysis Cassettes (10,000 weight cutoff; Thermo Fisher Scientific) at room temperature. These dialyzed proteins were used for all experiments in this study.

Crystallization and data collection

We crystallized Rv2613c and collected the diffraction data as described previously.[18] Briefly, SeMet-Rv2613c was crystallized by hanging-drop vapor diffusion. Specifically, 5 μL of protein (10 mg mL^{-1}) was mixed with 5 μL of crystallization solution [0.1 M sodium cacodylate (pH 6.7), 0.2 M lithium sulfate, and 28% polyethylene glycol 400], and then the drop was suspended on a siliconized coverslip over 0.6 mL of the crystallization solution. Prismatic colorless crystals of SeMet-Rv2613c

formed after about 4 weeks at 20 °C and grew to a maximum size of 0.5 mm. The crystals were harvested using a CryoLoop (Hampton Research, Aliso Viejo, CA) and flash cooled to 100 K in a nitrogen gas stream.

The diffraction data for SeMet-Rv2613c were collected at the AR-NW12A station of the Photon Factory (Tsukuba, Japan) at a wavelength of 0.97901 Å with an ADSC Quantum 210r detector (Area Detector Systems Corporation, Poway, CA) located 240 mm from the crystal in 2-s 1° oscillations at 100 K. The diffraction data were processed, merged, and scaled using the HKL2000 (DENZO and SCALEPACK) software package.[24]

Structure determination and model analysis

The crystal structure of Rv2613c was solved by using SAD. SAD phasing and phase refinement were performed by using the PHENIX software package.[25] We built a model of Rv2613c with the Coot program,[26] and then refined it with CCP4,[27] CNSsolve,[28] and PHENIX to 1.89 Å resolution. We validated the model by using MolProbity.[29]

Ribbon diagrams were generated by PyMOL,[30] and protein structure topology cartoons were produced by TopDraw.[31] The atomic coordinates of crystal structures were downloaded from PDB†. We searched for similar protein structures by using the Dali server‡[32] and performed pairwise structure comparisons with the DaliLite program.[33] Sequence alignments were performed by using CLUSTAL W 1.83.[34]

Enzyme activity assays

The enzyme activity of Rv2613c and its mutants was measured by using a high-performance liquid chromatography system (Shimadzu, Kyoto, Japan) to quantify the amount of remaining substrate after the reaction, as described previously,[4] with some modifications. The reaction mixture (100 μL) consisted of 50 mM Hepes-Na (pH 7.6), 1 mM $MnCl_2$, 100 μg mL^{-1} bovine serum albumin, 1 mM Ap_4A, 5 mM phosphate, and purified enzymes. This mixture was incubated at 37 °C for 30 min. The reaction was stopped by heating at 95 °C for 4 min, followed by centrifugation of the reaction solution at 12,000*g* for 3 min. The clear supernatant was analyzed using a 4.6 mm × 125 mm Partisphere 5-μm SAX HPLC column (Whatman, Kent, UK), which was equilibrated with pure water. The adsorbed nucleotides, such as AMP, ADP, ATP, and Ap_4A, were eluted with a gradient of water and elution buffer [1.3 M $(NH_4)_2HPO_4$ with H_3PO_4 (pH 4.8)] as follows: 0–10 min, 0% elution buffer; 10–110 min, 0–50% elution buffer at a flow rate of 0.5 mL min^{-1}. The eluted nucleotides were detected at 254 nm. One unit of enzyme activity was defined as the degradation of 1.0 μmol of Ap_4A in 1 min at 37 °C. K_m and K_{cat} values were calculated by using GraphPad Prism (GraphPad Software, La Jolla, CA). Results were expressed as the mean (standard error of the mean) of three independent measurements.

†www.rcsb.org
‡ekhidna.biocenter.helsinki.fi/dali_server

Accession codes

The structure factor and atomic coordinates for Rv2613c have been deposited in the PDB under accession code 3ANO.

Acknowledgements

We thank the beamline staff at the AR-NW12A station of the Photon Factory for their assistance with data collection. Synchrotron radiation experiments at this facility were performed as outlined in proposal nos. 2008G610 and 2010G520. This study was funded by grants from the Ministry of Health, Labor, and Welfare of Japan (grant H22-Shinkou-Ippan-007) and by a Grant-in-Aid for Young Scientists (B) from the Ministry of Education, Culture, Sports, Science and Technology of Japan (grant 20780066).

References

1. Korenromp, E. L., Bierrenbach, A. L., Williams, B. G. & Dye, C. (2009). The measurement and estimation of tuberculosis mortality. *Int. J. Tuberc. Lung Dis.* **13**, 283–303.
2. Chiang, C. Y. & Yew, W. W. (2009). Multidrug-resistant and extensively drug-resistant tuberculosis. *Int. J. Tuberc. Lung Dis.* **13**, 304–311.
3. Mori, S., Yamasaki, M., Maruyama, Y., Momma, K., Kawai, S., Hashimoto, W. *et al.* (2005). NAD-binding mode and the significance of intersubunit contact revealed by the crystal structure of *Mycobacterium tuberculosis* NAD kinase–NAD complex. *Biochem. Biophys. Res. Commun.* **327**, 500–508.
4. Mori, S., Shibayama, K., Wachino, J. & Arakawa, Y. (2010). Purification and molecular characterization of a novel diadenosine 5′,5‴-P^1,P^4-tetraphosphate phosphorylase from *Mycobacterium tuberculosis* H37Rv. *Protein Expression Purif.* **69**, 99–105.
5. Sassetti, C. M., Boyd, D. H. & Rubin, E. J. (2003). Genes required for mycobacterial growth defined by high density mutagenesis. *Mol. Microbiol.* **48**, 77–84.
6. Raman, K., Yeturu, K. & Chandra, N. (2008). targetTB: a target identification pipeline for *Mycobacterium tuberculosis* through an interactome, reactome and genome-scale structural analysis. *BMC Syst. Biol.* **2**, 109.
7. Brenner, C. (2002). Hint, Fhit, and GalT: function, structure, evolution, and mechanism of three branches of the histidine triad superfamily of nucleotide hydrolases and transferases. *Biochemistry*, **41**, 9003–9014.
8. Mulder, W., Scholten, I. H., van Roon, H. & Grivell, L. A. (1994). Isolation and characterization of the linked genes APA2 and QCR7, coding for Ap_4A phosphorylase II and the 14 kDa subunit VII of the mitochondrial bc_1-complex in the yeast *Kluyveromyces lactis*. *Biochim. Biophys. Acta*, **1219**, 719–723.

9. Plateau, P., Fromant, M., Schmitter, J. M. & Blanquet, S. (1990). Catabolism of bis(5'-nucleosidyl) tetraphosphates in *Saccharomyces cerevisiae*. *J. Bacteriol.* **172**, 6892–6899.
10. Huang, Y., Garrison, P. N. & Barnes, L. D. (1995). Cloning of the *Schizosaccharomyces pombe* gene encoding diadenosine 5′,5‴-P^1,P^4-tetraphosphate (Ap_4A) asymmetrical hydrolase: sequence similarity with the histidine triad (HIT) protein family. *Biochem. J.* **312**, 925–932.
11. Lima, C. D., Klein, M. G. & Hendrickson, W. A. (1997). Structure-based analysis of catalysis and substrate definition in the HIT protein family. *Science*, **278**, 286–290.
12. Pace, H. C., Garrison, P. N., Robinson, A. K., Barnes, L. D., Draganescu, A., Rosler, A. *et al.* (1998). Genetic, biochemical, and crystallographic characterization of Fhit–substrate complexes as the active signaling form of Fhit. *Proc. Natl Acad. Sci. USA*, **95**, 5484–5489.
13. Krakowiak, A., Pace, H. C., Blackburn, G. M., Adams, M., Mekhalfia, A., Kaczmarek, R. *et al.* (2004). Biochemical, crystallographic, and mutagenic characterization of Hint, the AMP-lysine hydrolase, with novel substrates and inhibitors. *J. Biol. Chem.* **279**, 18711–18716.
14. Geeganage, S., Ling, V. W. & Frey, P. A. (2000). Roles of two conserved amino acid residues in the active site of galactose-1-phosphate uridylyltransferase: an essential serine and a nonessential cysteine. *Biochemistry*, **39**, 5397–5404.
15. Barnes, L. D., Garrison, P. N., Siprashvili, Z., Guranowski, A., Robinson, A. K., Ingram, S. W. *et al.* (1996). Fhit, a putative tumor suppressor in humans, is a dinucleoside 5′,5‴-P^1,P^3-triphosphate hydrolase. *Biochemistry*, **35**, 11529–11535.
16. Guranowski, A. & Blanquet, S. (1985). Phosphorolytic cleavage of diadenosine 5′,5‴-P^1,P^4-tetraphosphate. Properties of homogeneous diadenosine 5′,5‴-P^1,P^4-tetraphosphate alpha, beta-phosphorylase from *Saccharomyces cerevisiae*. *J. Biol. Chem.* **260**, 3542–3547.
17. McLennan, A. G., Mayers, E., Hankin, S., Thorne, N. M., Prescott, M. & Powls, R. (1994). The green alga *Scenedesmus obliquus* contains both diadenosine 5′,5‴-P^1,P^4-tetraphosphate (asymmetrical) pyrophosphohydrolase and phosphorylase activities. *Biochem. J.* **300**, 183–189.
18. Mori, S., Shibayama, K., Wachino, J. & Arakawa, Y. (2010). Crystallization and preliminary X-ray analysis of the diadenosine 5′,5‴-P^1,P^4-tetraphosphate phosphorylase from *Mycobacterium tuberculosis* H37Rv. *Acta Crystallogr. Sect. F*, **66**, 279–281.
19. Mccoy, J. G., Arabshahi, A., Bitto, E., Bingman, C. A., Ruzicka, F. J., Frey, P. A. & Phillips, G. N. (2006). Structure and mechanism of an ADP-glucose phosphorylase from *Arabidopsis thaliana*. *Biochemistry*, **45**, 3154–3162.
20. McLennan, A. G., Barnes, L. D., Blackburn, G. M., Brenner, C., Guranowski, A., Miller, A. D. *et al.* (2001). Recent progress in the study of the intracellular functions of diadenosine polyphosphates. *Drug Dev. Res.* **52**, 249–259.
21. Hoyle, C. H. V., Hilderman, R. H., Pintor, J. J., Schluter, H. & King, B. F. (2001). Diadenosine polyphosphates as extracellular signal molecules. *Drug Dev. Res.* **52**, 260–273.
22. Ismail, T. M., Hart, C. A. & McLennan, A. G. (2003). Regulation of dinucleoside polyphosphate pools by the YgdP and ApaH hydrolases is essential for the ability of *Salmonella enterica* serovar Typhimurium to invade cultured mammalian cells. *J. Biol. Chem.* **278**, 32602–32607.
23. Monds, R. D., Newell, P. D., Wagner, J. C., Schwartzman, J. A., Lu, W., Rabinowitz, J. D. & O'Toole, G. A. (2010). Di-adenosine tetraphosphate (Ap_4A) metabolism impacts biofilm formation by *Pseudomonas fluorescens* via modulation of c-di-GMP-dependent pathways. *J. Bacteriol.* **192**, 3011–3023.
24. Otwinowski, Z. & Minor, W. (1997). Processing of X-ray diffraction data collected in oscillation mode. *Methods Enzymol.* **276**, 307–326.
25. Adams, P. D., Afonine, P. V., Bunkoczi, G., Chen, V. B., Davis, I. W., Echols, N. *et al.* (2010). PHENIX: a comprehensive Python-based system for macromolecular structure solution. *Acta Crystallogr. Sect. D*, **66**, 213–221.
26. Emsley, P., Lohkamp, B., Scott, W. G. & Cowtan, K. (2010). Features and development of Coot. *Acta Crystallogr. Sect. D*, **66**, 486–501.
27. Collaborative Computational Project, Number 4. (1994). The *CCP4* suite: programs for protein crystallography. *Acta Crystallogr. Sect. D*, **50**, 760–763.
28. Brunger, A. T., Adams, P. D., Clore, G. M., DeLano, W. L., Gros, P., Grosse-Kunstleve, R. W. *et al.* (1998). Crystallography & NMR System: a new software suite for macromolecular structure determination. *Acta Crystallogr. Sect. D*, **54**, 905–921.
29. Chen, V. B., Arendall, W. B., III, Headd, J. J., Keedy, D. A., Immormino, R. M., Kapral, G. J. *et al.* (2010). MolProbity: all-atom structure validation for macromolecular crystallography. *Acta Crystallogr. Sect. D*, **66**, 12–21.
30. The PyMOL Molecular Graphics System, Version 0.99, Schrödinger, LLC.
31. Bond, C. S. (2003). TopDraw: a sketchpad for protein structure topology cartoons. *Bioinformatics*, **19**, 311–312.
32. Holm, L. & Rosenstrom, P. (2010). Dali server: conservation mapping in 3D. *Nucleic Acids Res.* **38**, W545–W549.
33. Holm, L. & Park, J. (2000). DaliLite workbench for protein structure comparison. *Bioinformatics*, **16**, 566–567.
34. Thompson, J. D., Higgins, D. G. & Gibson, T. J. (1994). CLUSTAL W: improving the sensitivity of progressive multiple sequence alignment through sequence weighting, position-specific gap penalties and weight matrix choice. *Nucleic Acids Res.* **22**, 4673–4680.

Journal of Medical Microbiology (2011), 60, 582–591 DOI 10.1099/jmm.0.026047-0

Expression of the *Mycobacterium tuberculosis* PPE37 protein in *Mycobacterium smegmatis* induces low tumour necrosis factor alpha and interleukin 6 production in murine macrophages

Sylvia Daim, Ikuo Kawamura, Kohsuke Tsuchiya, Hideki Hara, Takeshi Kurenuma, Yanna Shen, Sita R. Dewamitta, Shunsuke Sakai, Takamasa Nomura, Huixin Qu and Masao Mitsuyama

Department of Microbiology, Kyoto University Graduate School of Medicine, Yoshida Konoe-cho, Sakyo-ku, Kyoto 606-8501, Japan

Correspondence
Ikuo Kawamura
ikuo_kawamura@mb.med.kyoto-u.ac.jp

Received 9 September 2010
Accepted 10 January 2011

PPE37 is a member of the *Mycobacterium tuberculosis* proline-proline-glutamic acid (PPE) multigene family. Its expression is upregulated in bacteria that are phagocytosed by macrophages and is enhanced even more in bacteria isolated from the lungs of infected mice. This raises the possibility that PPE37 may play a role in the virulence of *M. tuberculosis* and led to this investigation of the function of PPE37. Recombinant bacterial strains, one expressing the *M. tuberculosis* PPE37 protein (Ms_ppe37) and another harbouring the vector alone (Ms_vec) were generated from the non-pathogenic *Mycobacterium smegmatis*. These bacterial strains were used to infect peritoneal exudate and bone marrow-derived macrophages. It was found that, despite the comparable intracellular survival between the two recombinant *M. smegmatis* strains, Ms_ppe37 induced a significantly lower level of tumour necrosis factor alpha and interleukin 6 in the infected macrophages compared with Ms_vec. Western blot analyses revealed that the activation levels of nuclear factor kappa B, mitogen-activated protein kinase (MAPK)/extracellular signal-regulated kinase and MAPK/p38 were lower in macrophages infected with Ms_ppe37 than in macrophages infected with Ms_vec. These results suggest that PPE37 may have a potential role in interfering with the pro-inflammatory cytokine response of infected macrophages.

INTRODUCTION

The existence of the proline-proline-glutamic acid (PPE) multigene family was revealed when the decoding of the *Mycobacterium tuberculosis* genome was completed (Cole *et al.*, 1998). Members of this gene family were found to share a highly conserved N-terminal sequence of approximately 180 aa that also contained the conserved PPE motif. In contrast, their C-terminal regions were highly heterogeneous in both sequence and length (Cole *et al.*, 1998). The *ppe* genes are not found outside the genus *Mycobacterium* and are highly distributed among the pathogenic species of mycobacteria (Gey van Pittius *et al.*, 2006). For these reasons, they are speculated to contribute to the pathogenicity of *M. tuberculosis*. A possible functional role has been proposed for the PPE proteins, in which they serve as a source of antigenic variation that promotes antigenic diversity in *M. tuberculosis* (Cole *et al.*, 1998). Indeed, the PPE proteins reported to date are immunogenic, eliciting either humoral or T-cell immune responses (Choudhary *et al.*, 2003; Khan *et al.*, 2008; Romano *et al.*, 2008; Tundup *et al.*, 2008; Wang *et al.*, 2008).

One of the PPE proteins, PPE37, may have a role in the virulence of *M. tuberculosis*. It has been reported that expression of the *ppe37* gene is upregulated in *M. tuberculosis* during infection of murine bone marrow-derived macrophages (Schnappinger *et al.*, 2003; Voskuil *et al.*, 2004). Moreover, in *M. tuberculosis* isolated from the lungs of infected mice, expression of the *ppe37* gene is enhanced even more (Schnappinger *et al.*, 2003). Earlier studies have shown that an iron-dependent transcriptional regulator that is critical for proper iron homeostasis in *M. tuberculosis* regulates the expression of *ppe37* (Rodriguez *et al.*, 1999, 2002). When *M. tuberculosis* was exposed to iron-limiting conditions in *in vitro* culture, the expression of *ppe37* increased greatly (Rodriguez *et al.*, 2002; Schnappinger *et al.*, 2003). In addition, *in vitro* exposure of *M. tuberculosis* to nitrosative and oxidative growth conditions also increased the expression of *ppe37* (Schnappinger *et al.*, 2003; Voskuil *et al.*, 2004). Both of

Abbreviations: ERK, extracellular signal-regulated kinase; IL, interleukin; LDH, lactate dehydrogenase; MAPK, mitogen-activated protein kinase; MHC, major histocompatibility complex; NF-κB, nuclear factor kappa B; TNF-α, tumour necrosis factor alpha; TLR, Toll-like receptor.

these conditions are reported to mimic the macrophage phagosomal environment that contains *M. tuberculosis* (Schnappinger *et al.*, 2003). From these results, it seems that PPE37 is required for the adaptation of *M. tuberculosis* to the intracellular niche in macrophages.

In the present study, as a first step towards evaluating the possible role of PPE37 in the virulence of *M. tuberculosis*, we took advantage of the lack of *ppe* genes in *Mycobacterium smegmatis* and generated two recombinant bacterial strains using this non-pathogenic bacterium. Unlike the *M. tuberculosis* genome, which contains 69 *ppe* ORFs, the *M. smegmatis* genome contains only 2. Furthermore, none of the *M. smegmatis ppe* genes are orthologues of the *M. tuberculosis ppe37* gene (Gey van Pittius *et al.*, 2006). We cloned the *ppe37* gene from the *M. tuberculosis* strain H37Rv and expressed the gene in *M. smegmatis* strain mc^2 155 (Ms_ppe37). The ability of Ms_ppe37 to survive inside macrophages was assessed in *in vitro* infection of mouse macrophages. In addition, the effect of PPE37 on the macrophage cytokine response was also investigated.

METHODS

Bacterial strains and growth conditions. *Escherichia coli* DH5α was routinely grown in Lennox LB medium for use in DNA cloning procedures. *M. tuberculosis* strain H37Rv and *M. smegmatis* strain mc^2 155 were grown at 37 °C in Middlebrook 7H9 liquid medium or on Middlebrook 7H10 agar (Difco) supplemented with 0.5 % (w/v) albumin fraction V, 0.2 % (w/v) glucose, 0.5 % (v/v) glycerol and 0.05 % (v/v) Tween 80. For the preparation of culture filtrate fraction, recombinant *M. smegmatis* Ms_ppe37 was grown in Sauton medium as described by Rosenkrands & Andersen (2001). When required, 25 μg kanamycin ml^{-1} was also added.

Macrophages. C57BL/6 female mice of 7 to 9 weeks old (Japan SLC) were used in experiments according to protocols approved by the Animal Ethics and Research Committee of Kyoto University Graduate School of Medicine. Peritoneal exudate cells were harvested from mice 3–4 days after intraperitoneal injection with 2.5 ml 3 % (w/v) thioglycollate (Eiken Chemical). Cells were washed, seeded in tissue culture plates and cultured for 2 h in 5 % CO_2 at 37 °C in RPMI 1640 supplemented with 10 % (v/v) heat-inactivated fetal bovine serum. Adherent cells were used as peritoneal exudate macrophages after non-adherent cells had been removed by washing. In other experiments, bone marrow cells were collected from the tibiae of mice. Cells were cultured for 5–7 days in RPMI 1640 supplemented with 10 % heat-inactivated fetal bovine serum, 20 μg gentamicin ml^{-1} and 100 ng mouse macrophage colony-stimulating factor ml^{-1} (R&D Systems). After removal of non-adherent cells, adherent cells were used as bone marrow-derived macrophages.

Generation of recombinant *M. smegmatis* expressing PPE37. Chromosomal DNA was isolated from *M. tuberculosis*, and the *ppe37* gene was PCR-amplified with the use of forward primer 5′-TTACTAGTcaccatcacACCTTCCCGAT-3′ containing an *Spe*I site (underlined) and three His codons (lower-case letters), and reverse primer 5′-CCGTAAGCTTCTTCAACGTTTAATCTGACC-3′ containing a *Hin*dIII site (underlined). The PCR product of approximately 1.5 kb was cloned into the pEGFP vector (Clontech Laboratories), generating the recombinant plasmid pEGFP-his3ppe37. Three additional His codons were introduced at the 5′ end of the his3ppe37 sequence with the use of the same reverse primer and a second forward primer, 5′-TGAATTCATGcatcaccatcaccatcacACC-3′, containing an *Eco*RI site (underlined) and the His codons (lower-case letters). The resultant PCR product containing six consecutive His codons was inserted in frame into the cloning site of pMV261, a mycobacterial expression vector (Stover *et al.*, 1991), generating pMV261-his6ppe37. The recombinant plasmid or empty pMV261 was electroporated into *M. smegmatis* mc^2 155 according to standard procedures (Larsen, 2000). Recombinant *M. smegmatis* expressing 6His-tagged PPE37 (Ms_ppe37) and *M. smegmatis* harbouring empty pMV261 alone (Ms_vec) were selected on Middlebrook 7H10 agar containing 25 μg kanamycin ml^{-1}.

Detection of *ppe37* gene expression in recombinant *M. smegmatis*. Recombinant *M. smegmatis* strains were cultured until they reached an OD_{600} of 0.6–1.0 in 100 ml Middlebrook 7H9 liquid medium in the presence of 25 μg kanamycin ml^{-1}. Total bacterial RNA was isolated using Sepasol RNA I Super (Nacalai Tesque). All RNA samples were treated with DNase I (Promega) and subjected to PCR to test for the complete removal of genomic DNA. cDNA was synthesized from 1 μg total RNA in a 40 μl reaction mix containing reverse transcriptase buffer, 150 ng random primers, 2 μl 10 mM dNTP mix, 2 μl 0.1 M DTT and 400 U SuperScript III reverse transcriptase (Invitrogen). PCR was performed with a KOD-Plus enzyme kit (Toyobo) and the following primer pairs: (i) *ppe37* gene – 5′-TGTTGGACTGGTTCATCTCG-3′ (forward) and 5′-CAGTCTTGTTGCTTTGCTGG-3′ (reverse), product size 500 bp; and (ii) aminoglycoside phosphotransferase (*aph*) gene – 5′-AGGTAGCGTTGCCAATGATG-3′ (forward) and 5′-CTCACCGAGGCAGTTCCATA-3′ (reverse), product size 540 bp.

Detection of His-tagged PPE37. Recombinant *M. smegmatis* strains were cultured to an OD_{600} of 0.6–1.0 in 25 ml Middlebrook 7H9 liquid medium or 50 ml Sauton medium in the presence of 25 μg kanamycin ml^{-1}. Bacterial pellets were harvested, washed three times with ice-cold PBS and resuspended in extraction buffer containing 20 mM Tris/HCl (pH 6.8), 4 mM EDTA, 0.6 % SDS and protease inhibitor cocktail (Nacalai Tesque). Bacterial cells were disrupted and supernatants were collected after centrifugation at 20 000 *g* for 20 min at 4 °C. For preparation of the culture filtrate fraction, the culture supernatant of bacteria grown in Sauton medium was harvested by centrifugation at 2000 *g* for 15 min at 4 °C. The supernatant was filtered through a 0.2 μm syringe filter and concentrated to approximately 150 μl using a centrifugal filter with a cut-off value of 5 kDa (Millipore). Samples were subjected to SDS-PAGE, and the His-tagged PPE37 protein was detected by Western blotting and mouse anti-penta-His antibody (Qiagen). Chemiluminescent images were captured with a luminescent image analyser LAS-4000mini (Fujifilm).

***M. smegmatis* infection of macrophages.** Macrophages were seeded at 1×10^6 cells per well in 12-well tissue culture plates or at 3×10^5 cells per well in 24-well tissue culture plates. Cells were infected with Ms_ppe37 or Ms_vec at an m.o.i. of 20. At this m.o.i., the resulting infection rate was greater than 80 % as estimated in preliminary infection assays from microscopy evaluation of slides stained according to the Kinyon method (Chapin & Lauderdale, 2007). Four hours after infection, gentamicin was added to give a final concentration of 5 μg ml^{-1}. At 6, 24 and 48 h after infection, macrophages were washed and lysed in PBS containing 0.1 % (v/v) Triton X-100. Lysates were plated on Middlebrook 7H10 agar plates containing 25 μg kanamycin ml^{-1} and the number of intracellular bacteria was enumerated.

Assay for lactate dehydrogenase (LDH) release. Culture supernatants were harvested after infection of macrophages with Ms_ppe37 or Ms_vec for 6, 24 or 48 h. LDH activity in the culture supernatants

was assayed with an LDH cytotoxicity detection kit (Takara Bio). The percentage of LDH release was calculated as: percentage release=100 × (experimental LDH release−spontaneous LDH release)/(maximal LDH release−spontaneous LDH release). A value of maximal LDH release was obtained from culture supernatants of macrophages that were lysed with 1 % (v/v) Triton X-100.

Assay for cytokine production. Culture supernatants were harvested after infection of macrophages with Ms_ppe37 or Ms_vec for 24 h. The concentrations of cytokines in the culture supernatants were determined using commercially available ELISA kits for tumour necrosis factor alpha (TNF-α), interleukin 6 (IL-6), IL-1β (eBioscience) and IL-12p70 (Endogen). In some experiments, after infection of macrophages with Ms_ppe37 or Ms_vec for 3, 6, 9, 12 and 18 h, total RNA was extracted with a Nucleospin RNA II kit (Macherey-Nagel). RNA (250 ng) was treated with RNase-free DNase (Promega) and subsequently reverse transcribed into cDNA using a SuperScript VILO cDNA synthesis kit (Invitrogen). cDNAs were diluted tenfold, and a PCR was performed in an equal reaction volume using a KOD-Plus enzyme kit and the following primer pairs: (i) *tnf* gene – 5′-CATGAGCACAGAAAGCATGATCCG-3′ (forward) and 5′-TCTGGGCCATAGAACTGATGAGAG-3′ (reverse), product size 230 bp; (ii) *IL-6* gene – 5′-TTCCTCTCTGCAAGAGACT-3′ (forward) and 5′-TGTATCTCTCTGAAGGACT-3′ (reverse), product size 432 bp; and (iii) *Actb* gene – 5′-TGGAATCCTGTGGCATCCATGAAAC-3′ (forward) and 5′-TAAAACGCAGCTCAGTAACAGTCCG-3′ (reverse), product size 350 bp. Equal volumes of the PCR mixtures were electrophoresed in 1.5 % agarose gel, and DNA bands were visualized with ethidium bromide (2 μg ml^{-1}) staining.

Flow cytometric analysis. Macrophages were harvested after a 24 h infection with Ms_ppe37 or Ms_vec and treated with anti-CD16/CD32 mAb (clone 93; eBioscience) for 10 min. This was followed by a 20 min incubation on ice with one of the following phycoerythrin-conjugated antibodies against: major histocompatibility complex class I (MHC-I; clone 28-14-8), MHC-II (clone M5/114.15.2), B7.1 (CD80 clone 16-10A1), B7.2 (CD86, clone GL1) or CD40 (clone 1C10), or with an isotype control antibody (all from eBioscience). The intensity of each cell-surface marker was analysed on a FACScalibur flow cytometer equipped with CellQuest software (BD Biosciences).

Assay for nuclear factor-kappa B (NF-κB), extracellular signal-regulated kinase (ERK) and p38 phosphorylation. Macrophages were infected with Ms_ppe37 or Ms_vec for 0.5, 1, 2, 4, 6, 7 or 8 h. After infection, macrophages were lysed in buffer containing 10 mM Tris/HCl (pH 6.8), 1 % (v/v) NP-40 and proteinase/phosphatase inhibitor cocktail (Nacalai Tesque). Cell lysates were harvested and subjected to SDS-PAGE. Phosphorylated and unphosphorylated ERK and p38, as well as the phosphorylated p65 subunit of NF-κB, were detected in lots with specific antibodies (Cell Signaling Technology). β-Actin was detected with anti-β-actin antibody (Sigma-Aldrich). Chemiluminescent images were captured with a luminescent image analyser LAS-4000mini. In another experiment, macrophages were pre-treated with 20 or 40 μM U0126 (a MEK1/2 inhibitor; Cell Signaling Technology) or with 10 or 20 μM Calbiochem SB202190 (a p38 inhibitor; EMD Biosciences). On the basis of preliminary experiments, the inhibitors were used at the concentrations required to inhibit ERK and p38 activities. One hour after treatment, the macrophages were infected with Ms_ppe37 or Ms_vec. The culture supernatants were harvested 24 h after infection, and ELISA was performed to determine the concentrations of TNF-α and IL-6.

Statistical analysis. Data were analysed using Student's two-tailed *t*-test. Statistical significance was defined as a P value <0.05. Error bars represent SD.

RESULTS

Ms_ppe37 constitutively expresses *M. tuberculosis* PPE37 protein

In this study, we generated two recombinant *M. smegmatis* strains to investigate the effect of PPE37 on the macrophage response to bacterial infection. The Ms_ppe37 strain was engineered to express a 6His-tagged PPE37 protein from a recombinant pMV261 vector, whilst the Ms_vec strain harboured the vector alone. The pMV261 vector contains the kanamycin resistance gene *aph* for selection of transformed bacteria (Stover *et al.*, 1991). Both Ms_ppe37 and Ms_vec, which were grown in Middlebrook 7H9 medium in the presence of kanamycin, expressed the *aph* gene. However, only Ms_ppe37 was able to express the *ppe37* gene (Fig. 1a). Furthermore, Western blot analysis with anti-penta-His antibody detected a protein band representing PPE37 in the total cell lysate prepared from Ms_ppe37 but not from Ms_vec (Fig. 1b). These results confirmed that the transformation was successful and that *ppe37* gene expression was detectable only in *M. smegmatis* that had been electroporated with the recombinant vector. In addition, Western blot analysis also revealed that a protein band representing PPE37 was detectable in the total cell lysate but not in the culture filtrate fractions prepared from Ms_ppe37 grown in Sauton medium (Fig. 1c). This was not due to the absence of proteins in the culture filtrate fraction, as Coomassie blue staining revealed the presence of many protein bands in both the culture filtrate and the cell lysate fractions. From the result in Fig. 1(c), it could be suggested that PPE37 is not a secretory protein. We also compared the growth kinetics of Ms_ppe37 and Ms_vec in Middlebrook 7H9 medium, as excess production of recombinant protein is known to exert a metabolic burden on recombinant bacteria, sometimes reducing the growth of these cells (Bentley *et al.*, 1990). We observed no marked difference in the growth kinetics (Fig. 1d), indicating that expression of the *ppe37* gene did not influence the growth of Ms_ppe37.

PPE37 does not contribute to the intracellular survival of *M. smegmatis* in macrophages

M. smegmatis is inherently unable to multiply inside macrophages, and the number of intracellular bacteria decreased gradually after infection of macrophages *in vitro*. In order to determine whether PPE37 facilitated the intracellular survival of these bacteria in macrophages, we compared the survival kinetics of Ms_ppe37 and Ms_vec in peritoneal exudate macrophages by conducting a gentamicin protection assay. The results showed no significant difference in the number of bacteria between Ms_ppe37 and Ms_vec up to 48 h after infection (Fig. 2a). Similar results were also observed in bone marrow-derived macrophages (Fig. 2b). These results suggested that the presence of PPE37 was not able to enhance the intracellular survival of *M. smegmatis* in macrophages.

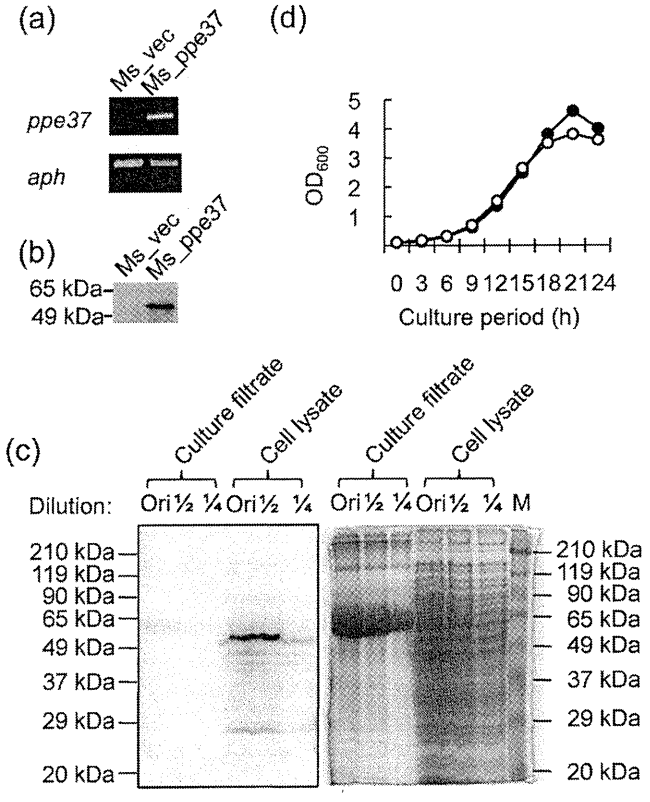

Fig. 1. Expression of *M. tuberculosis* PPE37 by *M. smegmatis* mc^2 155. (a) Ms_ppe37 and Ms_vec were grown at 37 °C in Middlebrook 7H9 liquid medium to an OD_{600} of 0.6–1.0. Total bacterial RNA was isolated and subjected to RT-PCR to detect expression of the *ppe37* and *aph* genes. (b) Lysates were prepared from bacterial cells that were cultured as in (a) and subjected to Western blot analysis to detect His-tagged PPE37 protein using mouse anti-penta-His antibody. (c) Lysate and culture filtrate fractions were prepared from Ms_ppe37 grown at 37 °C in Sauton medium to an OD_{600} of 0.6–1.0. Samples were diluted and subjected to Western blot analysis (left panel) as in (b), as well as to Coomassie blue staining (right panel), after SDS-PAGE. (d) Growth of Ms_ppe37 (○) and Ms_vec (●) at 37 °C in Middlebrook 7H9 liquid medium was monitored by determining OD_{600} at intervals of 3 h. Similar results were obtained in two independent experiments. Ori, Original undiluted sample; 1/2 and 1/4, samples diluted twofold and fourfold, respectively; M, protein marker.

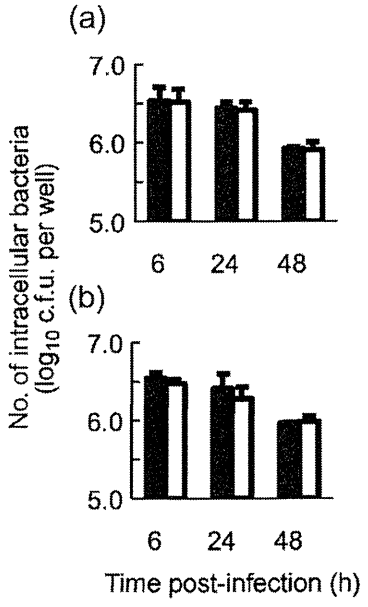

Fig. 2. Intracellular survival of recombinant *M. smegmatis* in macrophages. Peritoneal exudate macrophages (a) or bone marrow-derived macrophages (b) were infected with Ms_ppe37 (white bars) or Ms_vec (black bars) at an m.o.i. of 20. At 6, 24 and 48 h after infection, the macrophages were washed and lysed. Lysates were diluted and plated on Middlebrook 7H10 agar plates containing 25 μg kanamycin ml^{-1} to determine the number of c.f.u. Data are shown as means ± SD of triplicate wells. Similar results were obtained in three independent experiments.

PPE37 does not affect macrophage cell death during infection with *M. smegmatis*

One of the consequences of infecting host cells with *M. tuberculosis* is cell death, with the possibility that *M. tuberculosis* manipulates host-cell death as one of the mechanisms of pathogenicity. Recently, emerging new evidence prompted the proposal of a new model on the interaction between *M. tuberculosis* and its host cell (Behar *et al.*, 2010). This model suggests that, as a pathogenic strategy, virulent *M. tuberculosis* inhibits apoptosis whilst actively inducing necrosis in the infected host cell. The outcome of this strategy is a reduction in the efficiency of cross-presentation of mycobacterial antigens leading to the impairment in the initiation of T-cell immunity (Behar *et al.*, 2010; Divangahi *et al.*, 2010).

In this experiment, we thus wanted to determine whether PPE37 was able to affect the death of macrophages infected with *M. smegmatis*. Peritoneal exudate macrophages were infected with Ms_ppe37 or Ms_vec, and the amount of LDH released into the culture supernatant (an indicator of cell death) was determined. The result showed that macrophages infected with Ms_ppe37 or Ms_vec released a comparable amount of LDH (Fig. 3). In addition, microscopic examination also revealed no differences in the morphological features of the infected macrophages within the time period of infection (data not shown). Taken together, these results suggested that macrophage cell death was unaffected by PPE37 during infection with *M. smegmatis*.

Ms_ppe37 induces a lower level of pro-inflammatory cytokines in infected macrophages

To deduce the potential role of PPE37 in the virulence of *M. tuberculosis*, we investigated the effect that PPE37 might have on the immune response of infected macrophages. The aspect of the immune response that we examined first was cytokine production. Peritoneal exudate macrophages were

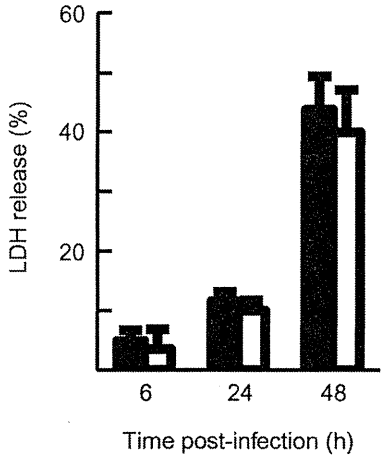

Fig. 3. Assay of cell death in macrophages infected with recombinant *M. smegmatis*. Peritoneal exudate macrophages were infected with Ms_ppe37 (white bars) or Ms_vec (black bars) at an m.o.i. of 20. At 6, 24 and 48 h after infection, culture supernatants were harvested. Release of LDH as a measure of macrophage cell death was estimated by assaying LDH activity in the culture supernatants. Data are shown as means ± SD of triplicate wells. Similar results were obtained in three independent experiments.

infected with Ms_ppe37 or Ms_vec for 24 h, and the concentrations of cytokines in the culture supernatants were determined. Consistent with the cytokine profiles reported elsewhere for macrophages infected with *M. smegmatis* (Lee & Schorey, 2005; Post *et al.*, 2001; Roach & Schorey, 2002), peritoneal exudate macrophages infected with Ms_vec or Ms_ppe37 also produced TNF-α, IL-6, IL12p70 and IL-1β (Fig. 4a–d). However, we discovered that Ms_ppe37 induced a significantly lower level of these cytokines in infected macrophages compared with Ms_vec. We repeated the infection experiment in bone marrow-derived macrophages, and measured the production of TNF-α and IL-6. Similar to infection in peritoneal exudate macrophages, Ms_ppe37 also induced a significantly lower level of TNF-α and IL-6 in the infected bone marrow-derived macrophages compared with Ms_vec (Fig. 4e, f). RT-PCR analyses showed that the expression of TNF-α mRNA in macrophages infected with Ms_ppe37 was delayed compared with the expression in macrophages infected with Ms_vec. The difference in the expression level was observed until 9 h after infection and thereafter became comparable (Fig. 4g). Although expression of IL-6 mRNA occurred much later, from 12 h after infection, the mRNA levels were also lower in macrophages infected with Ms_ppe37 than in macrophages infected with Ms_vec. However, despite the differential cytokine response, flow cytometric analysis revealed no significant differences in the expression levels of MHC-I, MHC-II, CD80, CD86 and CD40 between macrophages infected with Ms_ppe37 and macrophages infected with Ms_vec (Fig. 5). Taken together, these results suggested that PPE37 might possess a functional property that interferes with the pro-inflammatory cytokine production of macrophages infected with *M. smegmatis* but does not affect the expression of surface markers on these macrophages.

PPE37 alters the activation levels of NF-κB, ERK and p38 in macrophages infected with *M. smegmatis*

NF-κB is a major transcription factor responsible for the expression of both TNF-α and IL-6 mRNAs (Collart *et al.*, 1990; Faggioli *et al.*, 2004; Kuprash *et al.*, 1999; Libermann & Baltimore, 1990; Zhang *et al.*, 1994). It has been reported that NF-κB activation is needed to induce the expression of TNF-α and IL-6 mRNAs in macrophages infected with *M. smegmatis* (Gutierrez *et al.*, 2008). In addition, a previous study showed that *M. smegmatis* infection is also able to induce phosphorylation of the NF-κB p65 subunit (Lee & Schorey, 2005). The altered TNF-α and IL-6 mRNA expression shown in Fig. 4(g) therefore raised the possibility that NF-κB activation might be altered in macrophages infected with Ms_ppe37. To clarify this possibility, Western blot analysis was performed and the level of phosphorylated NF-κB p65 subunit in the infected macrophages was assessed. It was observed that Ms_ppe37 induced a relatively lower level of p65 phosphorylation in the infected macrophages compared with Ms_vec (Fig. 6a).

In addition to NF-κB, it has been shown that the expression of TNF-α mRNA in macrophages infected with *M. smegmatis* also requires the activation of p38 and ERK (Lee & Schorey, 2005; Roach *et al.*, 2005). Pharmacological inhibition experiments confirmed the requirement for ERK and p38 activities in the production of TNF-α and IL-6 in macrophages infected with Ms_vec (Fig. 6d, e). These results (Figs 4g and 6d, e) thus led us to investigate whether the activation of these mitogen-activated protein kinases (MAPKs) might also be affected in macrophages infected with Ms_ppe37. Western blot analysis was performed and the levels of phosphorylated ERK and p38 in the infected macrophages were assessed. Fig. 6(b, c) showed that Ms_ppe37 also induced a relatively lower level of ERK and p38 phosphorylation in infected macrophages compared with Ms_vec. The lower transcriptional activation of the TNF-α and IL-6 genes in macrophages infected with Ms_ppe37 therefore might have been due to a lower level of activation of NF-κB, ERK and p38. Taken together, these results further argue for the possibility of PPE37 interfering with the pro-inflammatory cytokine response of macrophages infected with *M. smegmatis*.

DISCUSSION

In the present study, the results suggested the possibility that the *M. tuberculosis* PPE37 protein might interfere with the pro-inflammatory cytokine response in infected macrophages. We found that TNF-α, IL-6, IL-12p70 and IL-1β were produced at significantly lower concentrations by macrophages infected with Ms_ppe37 compared with